Cell Reports

Article

Mitofusin 2 in Macrophages Links Mitochondrial ROS Production, Cytokine Release, Phagocytosis, Autophagy, and Bactericidal Activity

Graphical Abstract

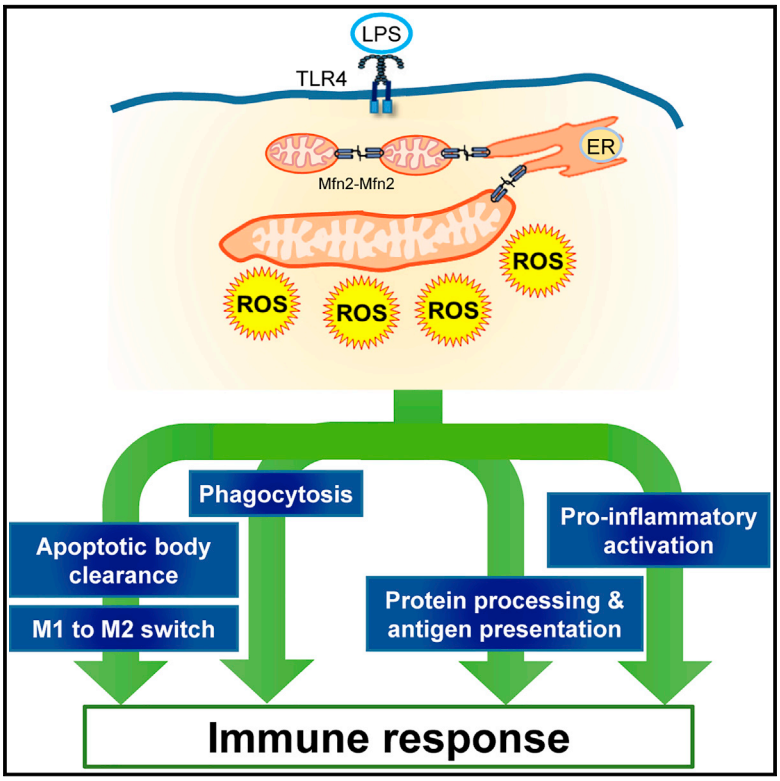

Authors

Juan Tur, Selma Pereira-Lopes, Tania Vico, ..., Antonio Zorzano, Jorge Lloberas, Antonio Celada

Correspondence

jlloberas@ub.edu (J.L.), acelada@ub.edu (A.C.)

In Brief

Tur et al. show that LPS-induced stress in macrophages requires mitofusin 2, which affects mitochondrial respiration and ROS production. The lack of Mfn2 in macrophages blocks the triggering of pro-inflammatory responses, phagocytosis, and antigen presentation.

Highlights

- In macrophages, LPS-induced ROS production requires mitochondrial mitofusin 2
- Mfn2 is required for the production of cytokines, phagocytosis, and antigen processing
- Survival from bacterial infection or septic shock is compromised in Mfn2$^{-/-}$ mice

Tur et al., 2020, Cell Reports *32*, 108079
August 25, 2020
https://doi.org/10.1016/j.celrep.2020.108079

CellPress

Cell Reports

CellPress
OPEN ACCESS

Article

Mitofusin 2 in Macrophages Links Mitochondrial ROS Production, Cytokine Release, Phagocytosis, Autophagy, and Bactericidal Activity

Juan Tur,[1] Selma Pereira-Lopes,[1] Tania Vico,[1] Eros A. Marín,[1] Juan P. Muñoz,[2,3,4] Maribel Hernández-Alvarez,[2,3,4] Pere-Joan Cardona,[5] Antonio Zorzano,[2,3,4] Jorge Lloberas,[1,6,*] and Antonio Celada[1,6,7,*]

[1]Macrophage Biology Group, Department of Cell Biology, Physiology and Immunology, Facultat de Biologia, Universitat de Barcelona, 08028 Barcelona, Spain

[2]Centro de Investigación Biomédica en Red de Diabetes y Enfermedades Metabólicas Asociadas (CIBERDEM), 08036 Barcelona, Spain

[3]Institute for Research in Biomedicine (IRB Barcelona), 08028 Barcelona, Spain

[4]Departament de Bioquímica i Biomedicina Molecular, Facultat de Biologia, Universitat de Barcelona, 08028 Barcelona, Spain

[5]Unitat de tuberculosi experimental, Institut Germans Trias i Pujol, Badalona, Spain

[6]Senior author

[7]Lead Contact

*Correspondence: jlloberas@ub.edu (J.L.), acelada@ub.edu (A.C.)

https://doi.org/10.1016/j.celrep.2020.108079

SUMMARY

Mitofusin 2 (Mfn2) plays a major role in mitochondrial fusion and in the maintenance of mitochondria-endoplasmic reticulum contact sites. Given that macrophages play a major role in inflammation, we studied the contribution of Mfn2 to the activity of these cells. Pro-inflammatory stimuli such as lipopolysaccharide (LPS) induced Mfn2 expression. The use of the *Mfn2* and *Mfn1* myeloid-conditional knockout (KO) mouse models reveals that Mfn2 but not Mfn1 is required for the adaptation of mitochondrial respiration to stress conditions and for the production of reactive oxygen species (ROS) upon pro-inflammatory activation. Mfn2 deficiency specifically impairs the production of pro-inflammatory cytokines and nitric oxide. In addition, the lack of Mfn2 but not Mfn1 is associated with dysfunctional autophagy, apoptosis, phagocytosis, and antigen processing. $Mfn2^{floxed;CreLysM}$ mice fail to be protected from *Listeria*, *Mycobacterium tuberculosis*, or LPS endotoxemia. These results reveal an unexpected contribution of Mfn2 to ROS production and inflammation in macrophages.

INTRODUCTION

Mitochondria are highly dynamic organelles that are in a continuous process of fusion and fission and constantly reshaping their morphology in response to cellular needs and functions. These dynamics influence the biology of mitochondria and play a crucial role in functions, such as apoptosis, autophagy, Ca^{2+} homeostasis, oxidative metabolism, and respiration (Liesa and Shirihai, 2013; Sebastián et al., 2017; Zorzano et al., 2015). In mammals, mitochondrial fusion is mediated by mitofusin 1 (Mfn 1), Mfn2, and optic atrophy 1 (Opa1) (Zorzano et al., 2010). In addition to its function in mitochondrial fusion, Mfn2 is also critical for the establishment of interactions between mitochondria and the endoplasmic reticulum (ER) (Bach et al., 2005; de Brito and Scorrano, 2008a; Sebastián et al., 2012; Zorzano et al., 2015).

The dysfunction of mitochondria and the ER underlie metabolic alterations. In this regard, Mfn2 is associated with obesity and type 2 diabetes in both humans and rodents (Bach et al., 2005; Sebastián et al., 2012; Zorzano et al., 2015). In addition, genetic mutations in *MFN2* cause Charcot-Marie-Tooth disease type 2A, a peripheral neuropathy (Bombelli et al., 2014; Verhoeven et al., 2006; Züchner et al., 2004). Mfn2 is involved not only in peripheral neuropathy but also in the function of hypothalamic neurons, a cell population that regulates food intake and energy homeostasis (Schneeberger et al., 2013). More recently, a connection between Mfn2 dysfunction, aging, and age-related muscular impairment has been reported (Sebastián et al., 2016).

Macrophages play a major role in regulating metabolism and inflammatory responses (Biswas and Mantovani, 2012). On the other hand, mitochondria are master regulators of metabolism but are also increasingly being recognized as central hubs for innate immune signaling (Tur et al., 2017; Weinberg et al., 2015; West et al., 2011b). Given the relevance of the link between Mfn2 and mitochondrial function, here, we addressed the role of this protein in the functional activity of macrophages in inflammation. There is only one previous report showing the relevance of Mfn2 in macrophages. In this study, Ichinohe et al. (2013) demonstrated, in an *in vitro* model using small interfering RNA (siRNA), the role of Mfn2 in inflammasome activation.

Macrophages play a critical role during immune response. Pro-inflammatory activators, such as lipopolysaccharide (LPS),

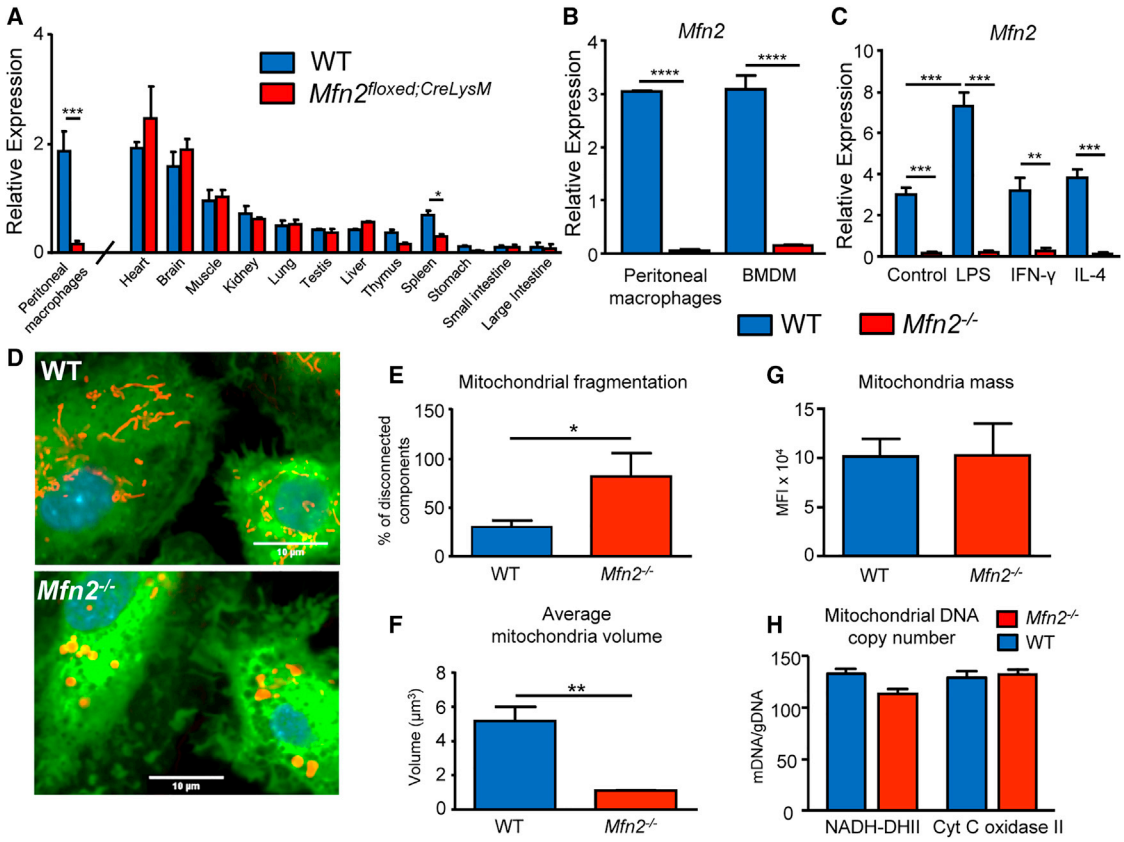

Figure 1. Mfn2 Is Highly Expressed in Macrophages, Is Induced by Pro-inflammatory Stimuli, and Is Required for Mitochondrial Integrity

(A) Mfn2 expression in different tissues compared to peritoneal macrophages, as well as in relation to Mfn2floxed$^{Cre+\ mice}$.

(B) Mfn2 expression in peritoneal macrophages and BMDMs, as well as in relation to Mfn2$^{-/-}$ macrophages.

(C) Mfn2 expression in activated BMDMs from WT and Mfn2$^{-/-}$ macrophages. LPS, IFN-γ, and IL-4 were added for 6 h at 10 ng/ml.

(D) Macrophage mitochondria stained with Mitotracker Deep Red (mitochondria), Calcein (cytoplasm), and Hoechst (nuclei) and observed by confocal fluorescence microscopy. Zooms of z stacks from images with at least 20 cells are shown. Bar, 10 μm.

(E) Quantification of the mitochondrial fragmentation degree.

(F) Quantification of the average volume for each "single" mitochondrion.

(G) Macrophage mitochondrial mass calculated by staining with Mitotracker Green.

(H) Number of mitochondrial DNA (mDNA) copies relative to the genomic DNA (gDNA).

All results are shown as mean ± SD from three independent experiments compared using two-way ANOVA; *p < 0.05, **p < 0.01, ***p < 0.001, ****p < 0.0001. Photographs are representative of five independent experiments. See also Figures S1–S3.

or interferon γ (IFN-γ) induce reactive oxygen species (ROS), a variety of molecules and free radicals derived from molecular oxygen that are essential mediators of the macrophage functional activities (Bodgan, 2001). The major source of ROS has been attributed to nitric oxide synthase (NOS) induced by pro-inflammatory activators (Bogdan, 2001).

Here, we provide evidence that macrophages require Mfn2 to adapt mitochondrial respiration and to produce ROS. Using a conditional mouse Mfn1$^{-/-}$, we demonstrate that the alterations detected in Mfn2-deficient macrophages are not due to reduced mitochondrial fusion but are instead to lower ROS production. The lack of ROS production results in defective extracellular signal-regulated kinase (ERK) and p38 signaling, which in turn reduces the production of pro-inflammatory cytokines and nitric oxide. In addition, Mfn2 deficiency is associated with dysfunctional autophagy, apoptosis, phagocytosis, and antigen processing. Our results unravel a key unexpected contribution of Mfn2 to ROS production and inflammation in macrophages.

RESULTS

Mfn2 Is Highly Expressed in Macrophages and Is Induced upon Pro-inflammatory Activation

Peritoneal and bone-marrow-derived macrophages (BMDMs) expressed high amounts of Mfn2, at similar levels to those found in the brain or the heart (Figures 1A and 1B). This high expression indicated that Mfn2 might play a relevant role in macrophage biology. Stimulation of macrophages with the Toll-like receptor (TLR) ligands LPS (TLR4), R848 (TLR7 and TLR8), and CpGB (TLR9) upregulated *Mfn2* expression (Figures 1C and S1A). However, *Mfn1* or *Opa-1* expression was not affected by LPS (Figures S1A and S1B), supporting the notion that Mfn2 and Mfn1,

despite being highly homologous, have different functions (Ishihara et al., 2004). Stimulation of the cells with the pro- (IFN-γ) or the anti-inflammatory cytokine (interleukin-4 [IL-4]) did not modify *Mfn2*, *Mfn1*, *or Opa1* expression (Figures 1C and S1B), indicating that the expression of *Mfn2* is specifically induced by TLR ligands.

To determine Mfn2 function in macrophages, we generated a myeloid-conditional KO mouse ($Mfn2^{floxed;\ Cre\text{-}LysM}$). In the BMDMs and peritoneal macrophages of this model, no *Mfn2* expression was detected, even under stimulation with TLR ligands (Figures 1A–1C). The deficiency in *Mfn2* did not modify the mRNA expression of Mfn1 or Opa1 (Figure S1B).

Characterization of $Mfn2^{-/-}$ Macrophages

BMDMs from wild-type (WT) and $Mfn2^{floxed;\ Cre+}$ mice show the same ability to respond to activation, proliferation, and apoptotic stimuli as the natural populations of monocytes and peritoneal macrophages (Celada et al., 1984). The morphology and the specific differentiation markers of the BMDMs from WT and $Mfn2^{floxed;\ Cre+}$ mice ($Mfn2^{-/-}$ hereafter) were similar (Figures S1C–S1E). Furthermore, the lack of *Mfn2* in these cells did not affect the number of circulating myeloid cells (Figure S1F).

In contrast to other cell types (Peng et al., 2015; Zhang et al., 2015), in the $Mfn2^{-/-}$ model, the proliferation and cell cycle progression of macrophages in response to macrophage colony stimulating factor (M-CSF) was independent of Mfn2 (Figures S2A–S2C). Also, markers of senescence, such as telomere shortening (Sebastián et al., 2009), were not found in these cells (Figure S2D).

Mfn2, in conjunction with Opa1 and Mfn1, regulates the morphology of the mitochondrial network by mediating fusion between adjacent organelles (de Brito and Scorrano, 2008b). To examine the effects of Mfn2 depletion on the morphology of mitochondria, we stained macrophages with the mitochondrial-specific dye MitoTracker Deep Red. Although WT macrophages presented a fused and filamentous mitochondrial network, with a higher average volume for each mitochondrion, $Mfn2^{-/-}$ macrophages showed highly fragmented mitochondria in the form of small spheres or short rods (Figures 1D, 1E, and S3A). These observations demonstrate that, as in other cell types (Chen et al., 2003; Hall et al., 2016; Sebastián et al., 2012), macrophages require Mfn2 to maintain a correct mitochondrial architecture.

Although the average volume of each mitochondrion was smaller in $Mfn2^{-/-}$ macrophages (Figure 1F), the total mitochondrial mass per cell, as determined by flow cytometry, was unaltered (Figure 1G). Furthermore, we extracted total DNA (nuclear and mitochondrial) from macrophages and measured the mitochondrial DNA (mDNA) copy number by qPCR. $Mfn2^{-/-}$ macrophages showed similar levels of mDNA compared to control macrophages (Figure 1H).

Mfn2 Deficiency Impairs Mitochondrial Membrane Potential and ROS Production

We then studied the effects of Mfn2 deficiency on mitochondrial function. $Mfn2^{-/-}$ macrophages showed a drastic reduction in mitochondrial membrane potential ($m\Delta\Psi$), and this was barely sensitive to cyanide m-chlorophenyl hydrazone (CCCP) treatment (Figures 2A and S3B).

Basal or ATP-coupled mitochondrial respiration of $Mfn2^{-/-}$ macrophages was not altered compared to WT counterparts (Figures 2B and 2C). However, the maximal respiratory capacity, obtained by disruption of the mitochondrial proton gradient with the uncoupler CCCP, was markedly diminished in $Mfn2^{-/-}$ macrophages (Figure 2B). The maximal mitochondrial respiratory capacity also allowed calculation of the spare respiratory capacity, which was decreased in Mfn2-deficient macrophages (Figure 2D). These results indicate that $Mfn2^{-/-}$ macrophages respire to their maximum capacity under basal conditions and are consequently unable to further increase their respiration rate in response to a metabolic challenge.

Given the impaired mitochondrial respiration in $Mfn2^{-/-}$ macrophages, we examined whether these cells showed increased glycolysis as a compensatory mechanism for the reduced respiratory capacity. To this end, we determined the extracellular acidification rate (ECAR) in real time. At baseline, no differences in ECAR were observed. To induce maximum glycolysis, we incubated macrophages with oligomycin A, which inhibits ATP synthase, thus stimulating the alternative generation of ATP by glycolysis. Even under this condition, maximal glycolysis was unaffected by Mfn2 deficiency (Figure 2E).

Macrophages were incubated with the red fluorescent dye MitoSox, which selectively stains mitochondrial ROS (mROS). In the absence of Mfn2, the production of mROS in macrophages was severely decreased under basal conditions and did not recover after LPS stimulation (Figures 2F and S3C). As a control, we treated cells with n-acetyl cysteine (NAC), which reduced LPS-induced ROS production to similar levels to those present in control and Mfn2-deficient cells.

In addition to mROS, we also measured total cellular ROS by using the fluorescent probe 2′7′-dichlorofluorescin diacetate (DCF-DA). This probe is not specific for a particular type of ROS and responds to all ROS activity within the cell, such as that of NADPH oxidases. Under basal conditions, $Mfn2^{-/-}$ macrophages also showed decreased cytoplasmic ROS, which was further accentuated after LPS stimulation (Figures 2G, S3D, and S3E).

In contrast, the expression of the antioxidant enzymes catalase and SOD2 was not affected by *Mfn2* deficiency (Figure 2H). This observation indicates that the decrease in ROS levels was due to a reduction in ROS production rather than to increased degradation.

To determine if the role of Mfn2 on ROS production is related to the mitochondrial fusion or to the ER-mitochondrial interactions, we generated a myeloid-conditional KO mouse, $Mfn1^{floxed;\ Cre\text{-}LysM}$. Although Mfn1 participates in mitochondrial fusion (Figure 2I) and shows an 80% similarity with Mfn2, these two proteins exert other activities that differ between them. In this regard, Mfn1 is not involved in ER-mitochondrial contacts. In BMDMs from $Mfn1^{-/-}$ animals, mROS was not altered in relation to the controls, even after LPS activation (Figure 2J).

Mfn2 Is Critical for Macrophage Pro-inflammatory Activation

The induction of pro-inflammatory genes by LPS in macrophages is mediated by a series of signaling transduction pathways, including mitogen-activated protein kinases (MAPKs)

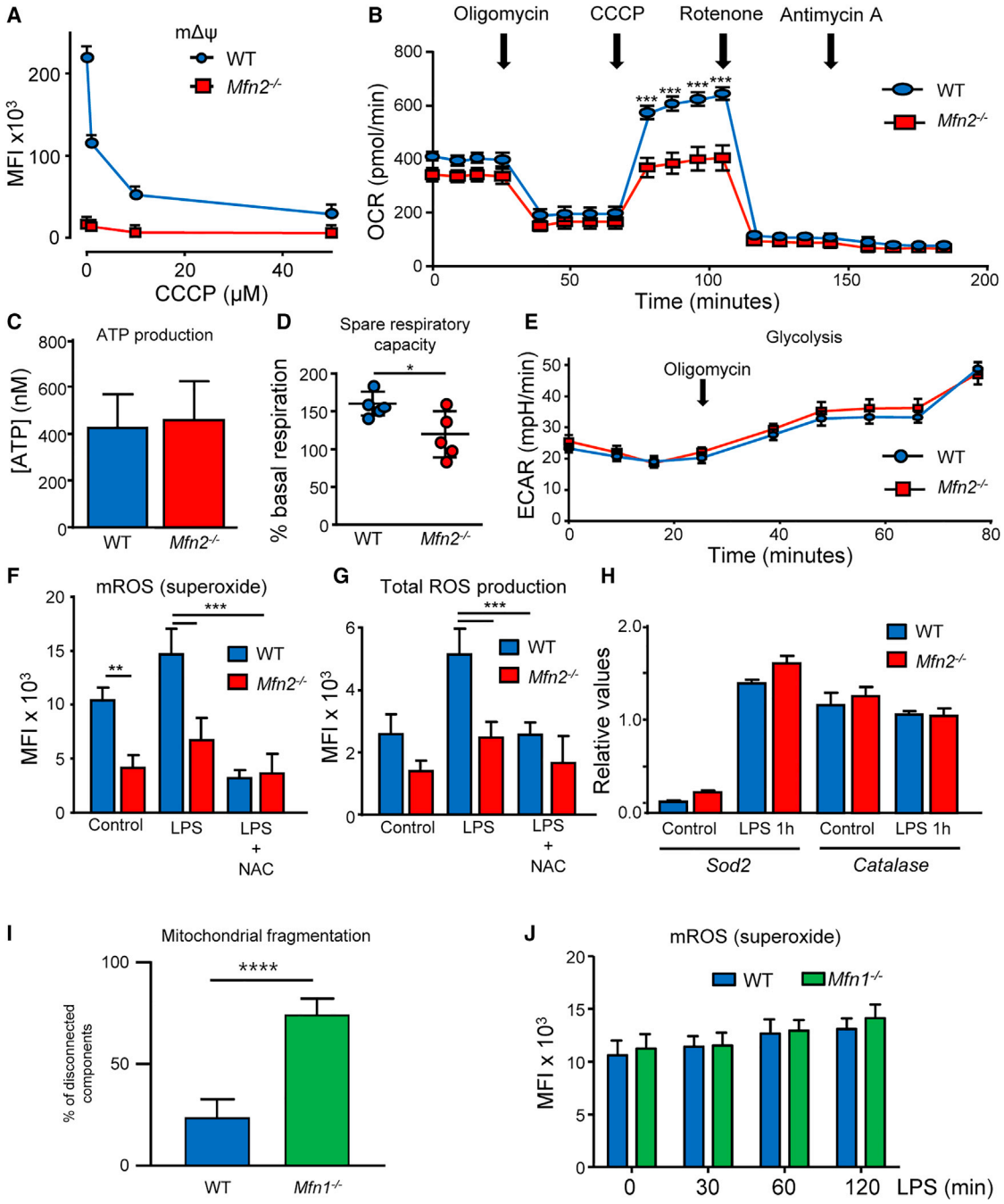

Figure 2. Mfn2 Is Required for Mitochondrial Respiration under Stress Conditions and for ROS Production

(A) Mitochondrial potential (mΔΨ). As a control, the proton uncoupler CCCP was used.

(B) Oxygen consumption ratio (OCR) of BMDMs was measured during sequential treatment with oligomycin (625 nM), CCCP, rotenone (1 μM), and antimycin A (1 μM).

(C) Quantification of ATP.

(D) Spare respiratory capacity.

(E) Glycolysis was calculated by measuring the extracellular acidification rate (ECAR) under basal conditions and after the addition of oligomycin.

(F) mROS was measured by MitoSox staining. Cells were treated with LPS (10 ng/ml) for 1 h or LPS with n-acetyl cysteine (NAC) (20 mM). Cells were incubated with NAC for 1 h before the LPS treatment.

(G) Total cellular ROS was measured by DCF-DA (50 μM) staining.

(H) Relative mRNA expression for catalase and Sod2 in control and LPS-stimulated BMDMs.

(I) mROS production in Mfn1$^{-/-}$. The results are from three to five independent experiments.

See also Figure S3.

(Lloberas et al., 2016). After LPS stimulation, the activation of the c-*jun* N-terminal kinase 1/2 (JNK1/2) in *Mfn2*$^{-/-}$ macrophages is indistinguishable from that of their WT counterparts (Figure S4A). However, the phosphorylation of p38 and ERK1/2 induced by LPS was significantly reduced in *Mfn2*$^{-/-}$ macrophages (Figures 3A and S4B). Furthermore, the LPS-induced activation of nuclear factor κB (NF-κB) also showed a moderate decrease in these cells (Figure 3B). These data confirm previous observations indicating that mROS production is required for NF-κB activation (Formentini et al., 2017).

As expected from the reduced activation of ERK1/2, p38, and NF-κB, the expression of pro-inflammatory cytokines *IL-1β*, *tumor necrosis factor α* (*TNF-α)*, *IL-6*, and *IL-12* was dramatically reduced in LPS-stimulated *Mfn2*$^{-/-}$ macrophages (Figure 3C). The production of TNF-α and IL-6 was reduced in Mfn2-deficient cells (Figures 3D and 3E). Furthermore, Mfn2 was also required for the normal expression of *Nos-2* and for the production of nitric oxide upon LPS stimulation (Figures 3C and 3F).

To determine the mechanism impairing the LPS-mediated induction of pro-inflammatory genes, we tested the expression of the MAPK phosphatase-1 (MKP-1), which dephosphorylates MAPKs in macrophages (Lloberas et al., 2016). The lack of Mfn2 did not affect the expression of MKP-1 (Figure S4C). Because ROS act as second messengers in the regulation of many signaling pathways, including MAPKs and NF-κB (Tur et al., 2017; West et al., 2011b), and the production of these radicals is disrupted in *Mfn2*$^{-/-}$ macrophages, we hypothesized that this lack of ROS mediates the impaired inflammatory activation. Macrophages treated for 1 h with the antioxidant NAC (which abolishes total cellular ROS) before LPS activation showed reduced p38 and ERK1/2 phosphorylation (Figures 3G and S4D), as well as a decreased induction of pro-inflammatory cytokines in response to LPS (Figure 3C). As a control, we used MitoTempo, a mROS-specific scavenger, which caused a dramatic repression of *Nos-2*, *TNF-α* ,and *IL-12* (Figure S4E). The expression of genes encoding *IL-1β*, *IL-6*, *TNF-α,* or *IFN-β*, and their response to LPS was not altered in Mfn1-deficient macrophages (Figure S5A).

ER stress responses, which can be regulated by Mfn2, may provide an alternative mechanism to explain the defect in inflammatory activation associated with Mfn2 deficiency (Bettigole and Glimcher, 2015; Hotamisligil, 2010), (Muñoz et al., 2013; Ngoh et al., 2012). We stimulated macrophages with either LPS or thapsigargin, a drug that induces ER stress by blocking Ca^{2+} channels at the ER. Among the ER-stress-associated genes determined, *Gadd34* and *Wfs1* expression showed a significant difference between WT and *Mfn2*$^{-/-}$ macrophages (Figure S3H). Therefore, we cannot exclude the participation of ER stress responses in the modulation of pro-inflammatory activation by Mfn2. No differences in ER-stress-associated genes were observed between WT and *Mfn1*$^{-/-}$ macrophages (Figure S5B).

The observation that Mfn2 is required for ROS production—a process that is required for the regulation of macrophage pro-inflammatory activity—prompted us to study whether this protein is also involved in anti-inflammatory activation. With the exception of *Ym1* (chitinase-3-like), stimulation of *Mfn2*$^{-/-}$ macrophages with IL-4 revealed no differences in the expression of anti-inflammatory-related markers, such as *Arginase1*, *Mannose receptor*, and *Fizz1* (resistin-like α) (Figure S5C). In addition, the enzymatic activity of arginase-1 showed no significant differences between WT and *Mfn2*$^{-/-}$ cells (Figure S5D). Finally, the phosphorylation of Stat6, the major signaling transduction pathway of IL-4, was not affected in the absence of Mfn2 (Figure S5E).

These results confirm that Mfn2 is necessary for the correct pro-inflammatory activation of macrophages and suggest that the associated reduction of ROS production may underlie the defect in the pro-inflammatory activation of Mfn2$^{-/-}$ macrophages.

Mfn2 Is Required in a Non-septic Inflammation Model

To determine whether the defects in inflammation observed in Mfn2$^{-/-}$ macrophages are translated *in vivo*, we used dinitrofenolbenzene (DNFB)-induced ear irritation as a model of sterile inflammation (Pereira-Lopes et al., 2015). In this model, the irritant DNFB was applied to the mouse ear. Monocytes migrate from the bloodstream to the damaged ear, where they differentiate into macrophages. These recruited macrophages play a major role in both the initiation and resolution of the inflammation (Bonneville et al., 2007).

At day 10 after treatment, the weight and thickness of the inflamed ears were significantly higher in WT mice than in *Mfn2*$^{floxed;\ Cre\text{-}LysM}$ animals (Figures 4A and 4B). Likewise, the expression of the pro-inflammatory cytokines *TNF-α*, *IL-6*, and *IL-1β* in the inflamed ears was higher in WT mice (Figure 4C). No inflammation was observed in the ears of the controls (i.e., treated with vehicle alone). These data demonstrate that macrophages require Mfn2 to generate a strong and efficient inflammatory response in a non-septic environment.

Mfn2 Is Involved in Autophagy, Phagocytosis, and Antigen Processing

Mitochondrial fusion and Mfn2 are intrinsically interlinked within the mitochondrion life cycle, a process that includes mitochondrial biogenesis and mitophagy (Song and Dorn, 2015; Soriano et al., 2006; Youle and van der Bliek, 2012). Mitochondria fuse to complement damaged components. But, when a single mitochondrion is damaged beyond repair, it is targeted by the autophagy machinery for degradation, thus preventing re-fusion to other mitochondria. If mitochondria do not fuse, the damage cannot be repaired and the organelle is targeted by autophagy (Twig et al., 2008; Youle and van der Bliek, 2012), which is also modulated by Mfn2 (Ding et al., 2015; Song and Dorn, 2015).

We evaluated autophagy by measuring the levels of the lipidated form of LC3 (LC3-II), which is associated with autophagosome formation. LC3-II levels were higher in *Mfn2*$^{-/-}$ macrophages than in control cells under basal conditions (Figures 5A and 5B). LPS treatment of *Mfn2*$^{-/-}$ macrophages caused LC3-II expression to decrease to the levels of unstimulated WT cells. This decrease is possibly attributable to an increase in lysosomal activity. However, autophagosome formation in WT macrophages was not affected by LPS stimulation (Figures 5A and 5B). Treatment with bafilomycin A1, an inhibitor of autophagosome-lysosome fusion, increased LC3-II levels in unstimulated and LPS-stimulated WT cells, as well as in LPS-stimulated *Mfn2*$^{-/-}$ macrophages. However, this treatment failed to further

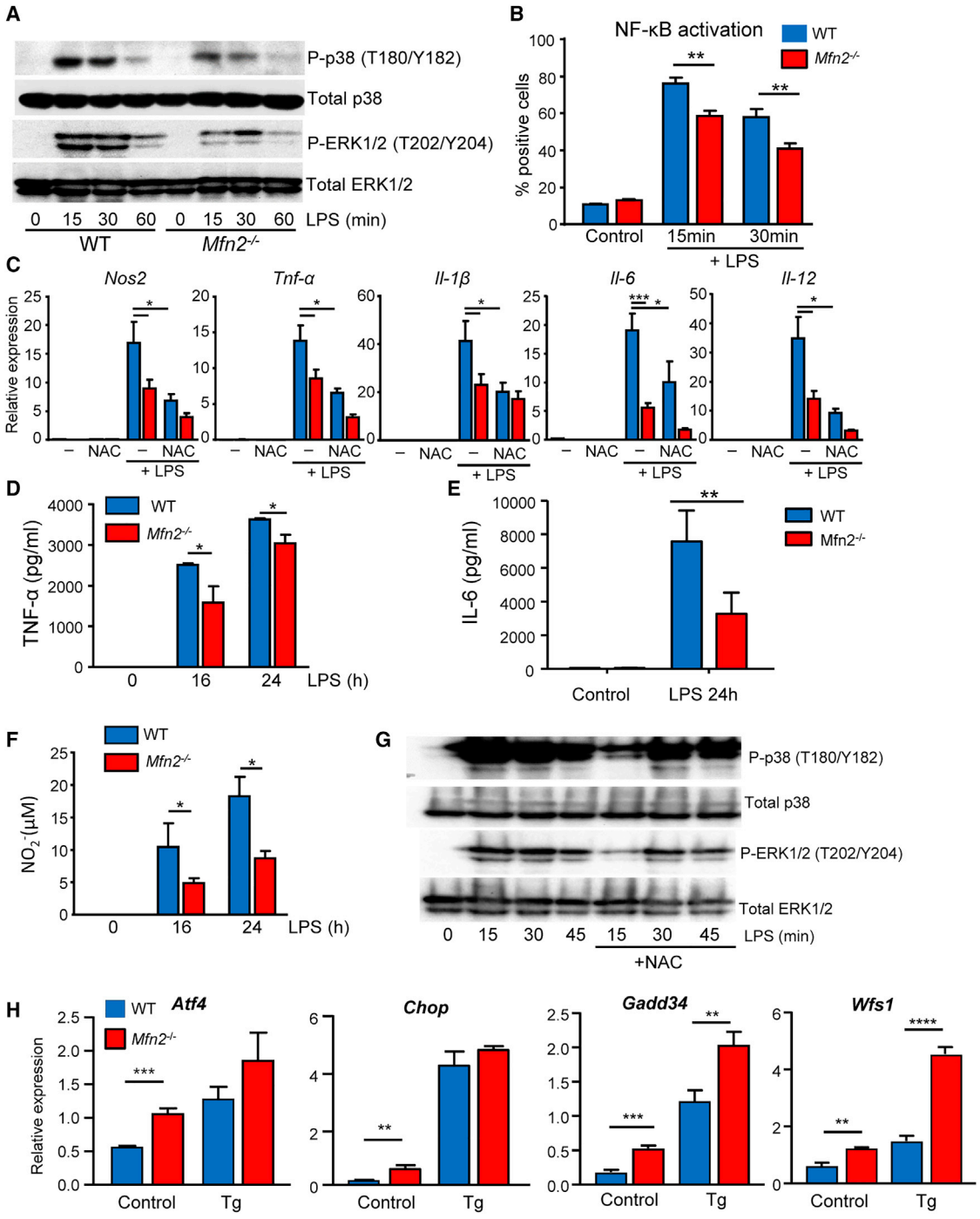

Figure 3. Pro-inflammatory Macrophage Activation Is Impaired in the Absence of Mfn2

(A) Cells were incubated with LPS (10 ng/ml) for the indicated times, and phosphorylation of p38 and ERK1/2 was measured.

(B) NF-κB activation was measured as the phosphorylation of p65 subunit.

(C) mRNA expression of pro-inflammatory cytokines in basal conditions after 3 h of LPS stimulation with or without previous treatment with NAC.

(D and E) TNF-α and IL-6.

(F) Levels of nitric oxide (NO).

(G) WT BMDMs were treated or not with NAC before the LPS treatment, and phosphorylation was measured.

(H) Control and *Mfn2*$^{-/-}$ macrophages were treated with thapsigargin (Tg) (3 μM) for 24 h, and then the gene expression was determined by qPCR. All results are from three independent experiments. See also Figures S4 and S5.

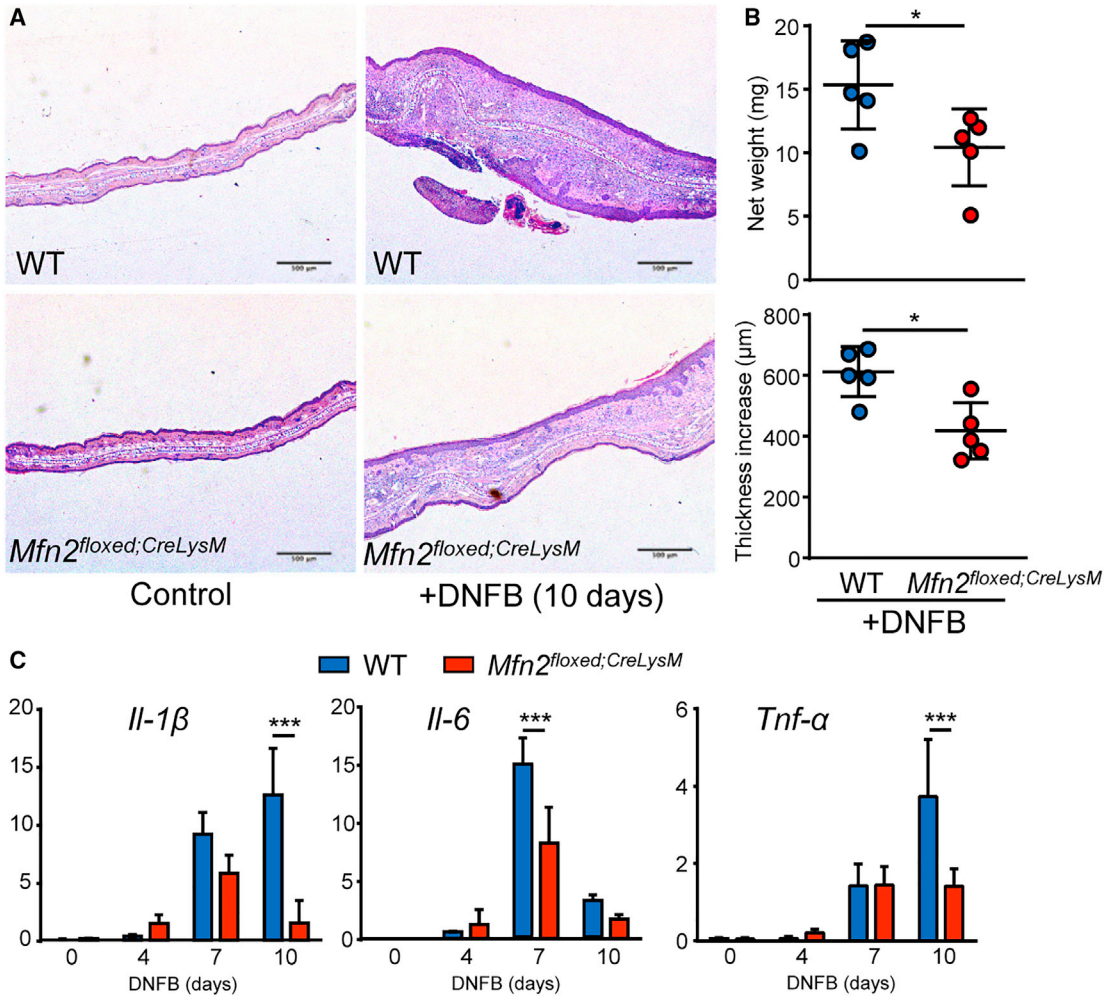

Figure 4. Mfn2 Is Required in a Non-septic Model of Inflammation

(A) Hematoxylin and eosin staining of ear sections at day 10. Scale bar 500 μm.

(B) Ear net weight and thickness at day 10.

(C) mRNA expression of DNFB-treated ears. The images and results are representative of two independent experiments each with five mice per group.

enhance the already high levels of LC3-II in *Mfn2*$^{-/-}$ macrophages, and therefore, their autophagic flux decreased compared to WT cells (Figures 5A and 5C). Altogether, these data demonstrate that Mfn2 maintains autophagy and that in the absence of this process autophagosomes accumulate and autophagic flux is markedly diminished.

There is a close relationship between autophagy and apoptosis (Mariño et al., 2014). A comparison of WT and *Mfn2*$^{-/-}$ macrophages revealed a similar percentage of apoptotic cells under basal conditions. However, after LPS stimulation, *Mfn2*$^{-/-}$ macrophages showed a significant increase in apoptosis compared to WT counterparts (Figure 5D).

Autophagy is also related to phagocytosis (Hurley and Young, 2017). We therefore examined whether in this critical function Mfn2 was also involved. The removal of apoptotic bodies by macrophages is an important process through which tissue homeostasis is maintained (Poon et al., 2014). *Mfn2*$^{-/-}$ macrophages failed to properly phagocytose apoptotic bodies from murine thymocytes (Figures 5E and S6A). Pre-stimulation with cytochalasin D, which depolymerizes actin and inhibits phagocytosis, abolished apoptotic body uptake in both WT and *Mfn2*$^{-/-}$ macrophages, thereby confirming that the differences observed were due to phagocytosis and not only to the binding of apoptotic bodies to the cellular membrane (Figures 5E and S6A).

In the absence of Mfn2, macrophages infected with the GFP-expressing *Aeromonas hydrophila*, a Gram-negative bacterium, showed a decrease in phagocytosis, as determined by both flow cytometry and colony-forming unit (CFU) quantification from macrophage lysates after 1 h of incubation (Figures 5F and 5G). This decrease was also confirmed using pHrodo-conjugated *Escherichia coli* (Gram negative) (Figure 5H) and *Staphylococcus aureus* (Gram positive) (Figure S6B). Furthermore, the phagocytic capacity of WT macrophages treated with NAC for 1 h decreased, reaching levels similar to those of *Mfn2*$^{-/-}$ macrophages (Figures 5H and S6B). This observation points to the involvement of ROS in the phagocytosis of bacterial pathogens.

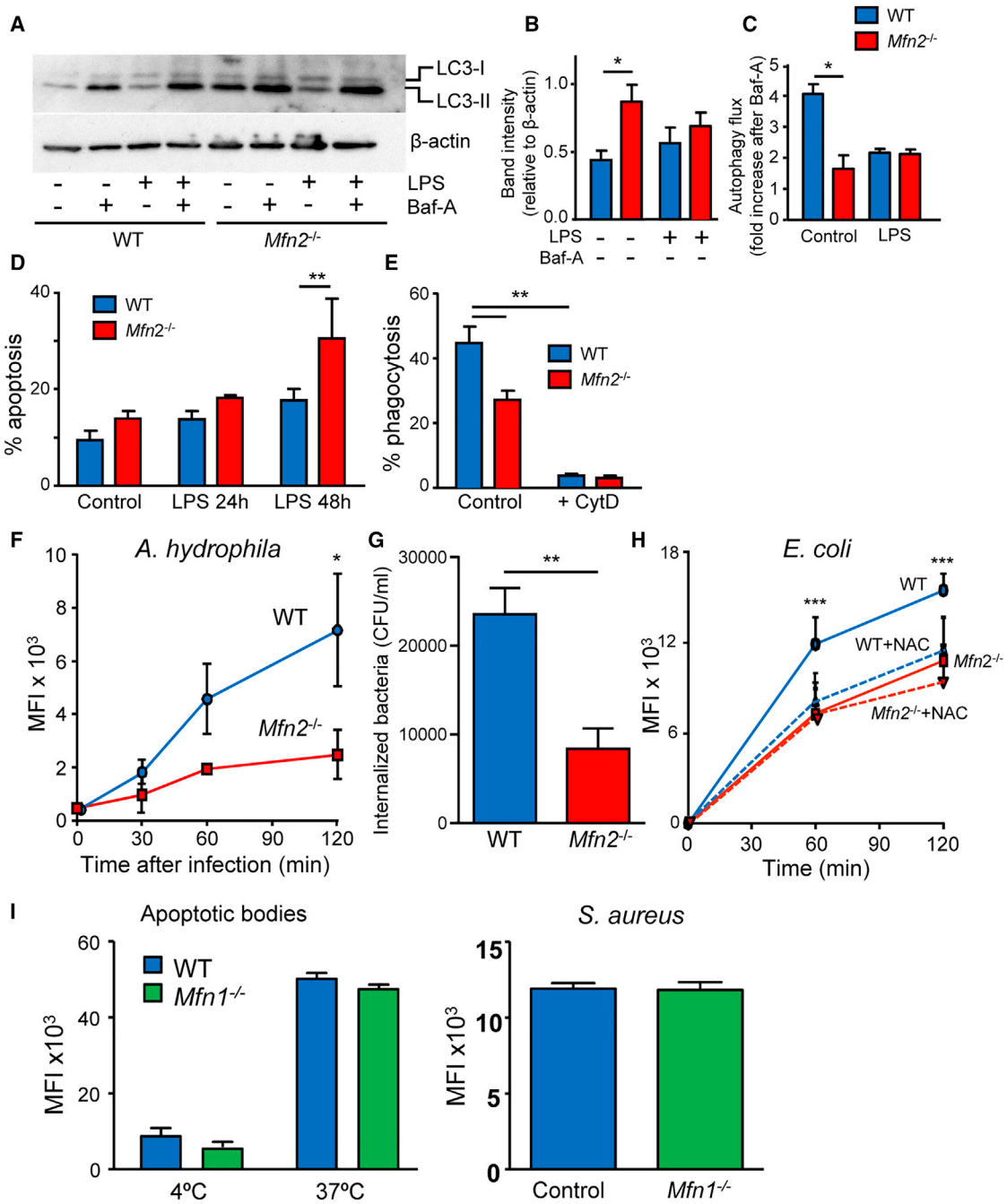

Figure 5. Mfn2 Is Essential for Autophagy, Apoptosis, and Phagocytosis

(A) Autophagy was measured by western blot of the lipidated form of LC3 (LC3-II) under basal conditions or under stimulation with LPS (10 ng/ml), and/or bafilomycin A (BafA) at 50 nM. Results are representative of four independent experiments.

(B) LC3-II in relation to β-actin.

(C) Autophagic flux as the fold increase in band intensity in BafA conditions to without BafA.

(D) Apoptosis.

(E) Phagocytosis of apoptotic bodies in BMDMs treated with or without cytochalascin D (2 μg/ml).

(F) Mean fluorescence intensity (MFI) showing BMDM phagocytosis of GFP-expressing *Aeromonas hydrophila*.

(G) CFU count of BMDM lysates 1 h after infection with *Aeromonas hydrophila*.

(H) Phagocytosis of pHrodo-conjugated *Escherichia coli* by BMDMs. Cells were treated for 1 h with NAC before bacteria were added and phagocytosis performed.

(legend continued on next page)

The levels of LC3-II were similar in control and Mfn1$^{-/-}$ macrophages under basal conditions and after LPS or bafilomycin A1 treatment (Figures S6C and S6D). In addition, the phagocytosis of apoptotic bodies or *Staphylococcus aureus* was not altered in *Mfn1*$^{-/-}$ macrophages (Figure 5I). All these data support the involvement of ROS in the phagocytic activity of *Mfn2*$^{-/-}$ macrophages.

In recent years, autophagy and phagocytosis have been postulated to be inter-regulated processes (Tur et al., 2017). The proposed mechanism to explain this relationship involves p62/sequestosome1, a protein required for autophagosome formation that is induced by LPS. When not sequestered in the autophagosome, this protein activates nuclear protein (erythroid-derived 2)-like 2 (NFE2L2), a transcription factor required for the expression of two class A scavenger receptors, namely macrophage receptor with collagenous structure (MARCO) and macrophage scavenger receptor-1 (MSR1), which are both required for phagocytosis (Bonilla et al., 2013). In both untreated and LPS-treated *Mfn2*$^{-/-}$ macrophages, the expression of class A scavenger receptors was decreased (Figure 6A). This observation suggests that Mfn2 participates in the LPS induction of MARCO and MSR1. The receptors detect both Gram-positive and Gram-negative bacteria, as well as other targets, such as apoptotic bodies, and their interaction with the corresponding ligand induces the phagocytosis of the bound target (Peiser et al., 2000).

The MARCO promoter contains antioxidant response elements that mediate the effect of NFE2L2 (or NRF2) (Harvey et al., 2011). We determined the expression of NRF2 under basal conditions and LPS stimulation. This factor was decreased in *Mfn2*$^{-/-}$ macrophages when compared to the controls (Figure 6B). These results could explain the low levels of scavenger receptors, MARCO and MSR1, and also the reduced phagocytosis associated with Mfn2 deficiency.

The Lack of Mfn2 Is Associated with Defective Bactericidal Activity and Protein Processing

So far, our results reveal that Mfn2 plays a major role in the phagocytosis of both bacteria and apoptotic bodies. Next, we studied whether Mfn2 is also involved in the degradation of phagocytosed bacteria. To this end, we performed a gentamycin protection assay to eliminate non-phagocytosed bacteria. CFUs were counted from macrophage lysates at various time points. After 24 h of phagocytosis, a drastic reduction in the number of CFUs was observed in both WT and *Mfn2*$^{-/-}$ macrophages, thereby indicating bacterial degradation (Figure S6E). Macrophage bactericidal activity was calculated as the percentage of initial bacteria that survived after 24 h. Bacteria phagocytosed by WT macrophages showed a marked decrease in survival compared to *Mfn2*$^{-/-}$ macrophages (Figure 6C). This observation thus indicates impaired bactericidal activity of the latter.

As antigen-presenting cells, macrophages can also trigger adaptive immune responses. To measure this functional activity, macrophages were pre-stimulated for 24 h with IFN-γ and then pulsed with either the full listeriolysin O (LLO), a major virulence factor of *Listeria monocytogenes*, or an 11-amino-acid pre-processed peptide of the same protein (190-201 LLO). The cells were then washed and incubated with a CD4^{+} T cell hybridoma with specificity for 190-201 LLO. The supernatants of these cultures were collected and incubated with a cell line that grows in an IL-2-dependent manner. Proliferation was then measured. *Mfn2*$^{-/-}$ macrophages processed and presented LLO, albeit somewhat less efficiently than WT macrophages (Figure 6D). However, no defect was observed when we used the peptide 190-201 LLO (Figure 6E). This observation suggests that the processing of the LLO protein, but not the antigen presentation itself, was impaired in *Mfn2*$^{-/-}$ macrophages. In addition, MHC-II expression was measured after incubation of macrophages with INF-γ. The expression of this marker was slightly decreased in *Mfn2*$^{-/-}$ macrophages and probably has no biological relevance (Figure S6F).

Mfn2 Is Required for the Immune Response to *Listeria monocytogenes*, *Mycobacterium tuberculosis*, and LPS Endotoxemia

To address the role of Mfn2 in immune responses *in vivo*, we studied murine infection with *Listeria monocytogenes*. This microorganism is a Gram-positive facultative intracellular bacterium with a preference to infect macrophages, and it grows preferentially in the spleen and liver. The *L. monocytogenes* intraperitoneal infection model is a rapid and quantitative assay, either by enumeration of liver and spleen CFUs or by monitoring the survival of infected animals (Portnoy et al., 2002).

We infected mice intraperitoneally and monitored their survival until the mice started recovering weight. The time course of the disease was similar in both groups; mice started to die at day 4, with the highest mortality observed at day 5 post-inoculation. At day 11, all the surviving mice from both groups started to recover body weight. However, the survival of *Mfn2*$^{floxed;\ Cre\text{-}LysM}$ mice was severely reduced compared to WT counterparts, reaching a significant decrease of more than 40% (Figure 7A). Another group of mice was infected with this bacterium and was sacrificed 48 h later to obtain spleen and liver samples. The early stage of innate resistance in *Mfn2*$^{floxed;\ Cre\text{-}LysM}$ animals was clearly affected, as noted by the marked increase in bacterial counts at 48 h (Figure 7A). This observation thus indicates that these mice were unable to control the infection.

To understand the molecular mechanisms involved in the dysfunctional immune responses to listeria, we infected BMDMs *in vitro* with *Listeria monocytogenes*. In *Mfn2*$^{-/-}$ macrophages, the expression of *TNF-*α and *IL-1*β was reduced (Figure S7A), suggesting that these cells failed to generate normal levels of pro-inflammatory cytokines in response to this infection.

We also used an *in vivo* mouse model of infection with *Mycobacterium tuberculosis* by using a sub-lethal dose of mycobacteria. Under these conditions, all WT mice survived the infection. However, the survival of the *Mfn2*$^{floxed;\ Cre\text{-}LysM}$ group was severely decreased, with merely 50% living by the end of the

(I) Phagocytosis of apoptotic bodies was measured as in (E), incubating cells and apoptotic bodies for 2 h at 37°C or at 4°C (negative control). Phagocytosis of *S. aureus* was measured as in (F), incubating cells and bacteria for 2 h at 37°C. Results are shown from at least three independent experiments.
See also Figure S6.

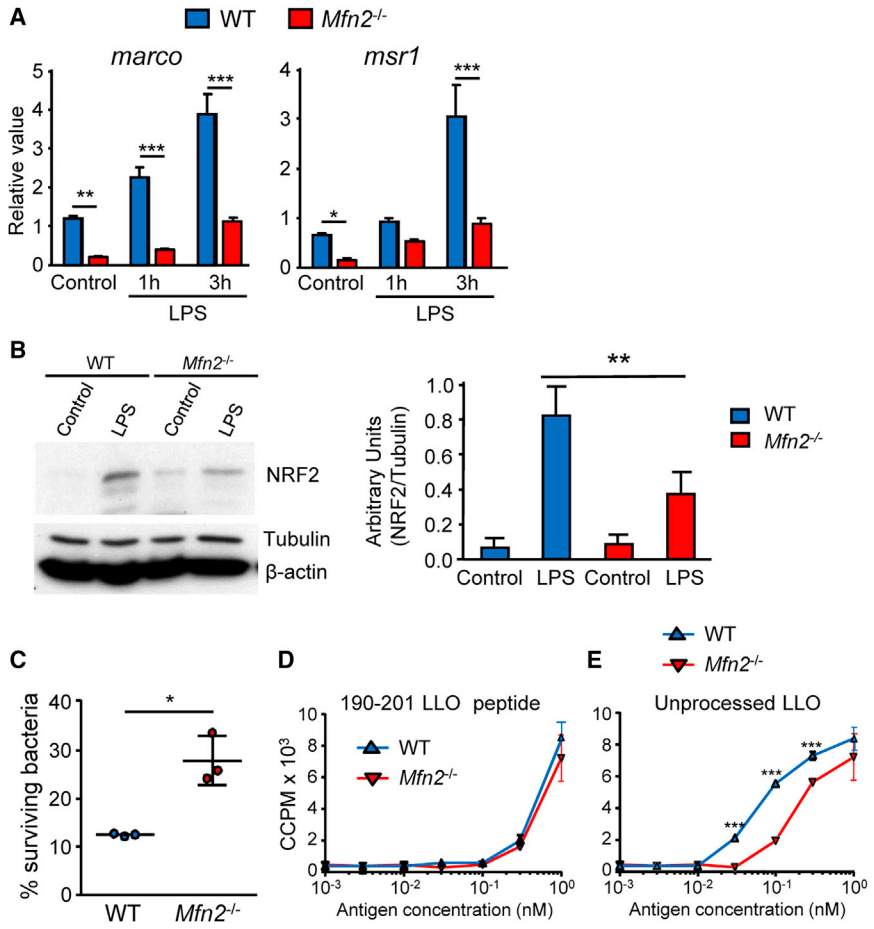

Figure 6. Mfn2 Is Critical for Protein Degradation

(A) The expression of class A scavenger receptors Marco and Msr1.

(B) NRF2 determined by western blot and quantification of three independent experiments.

(C) BMDMs phagocyted *Aeromonas hydrophila* for 1 h, and then non-phagocyted bacteria were removed with a gentamycin treatment (300 μg/ml) for 1 h. BMDMs were incubated at 37°C, and lysed at 24 h. The percentage of the surviving bacteria at 24 h relative to the initial CFU count is shown.

(D) Antigen presentation of the LLO full protein by IFN-γ stimulated (10 ng/ml for 24 h) BMDMs. Cells were pulsed with the full listeriolysin O (LLO) at the indicated concentrations. Macrophages were washed and incubated with a $CD4^+$ T cell hybridoma with specificity for 190-201 LLO. The supernatants were collected and incubated with a cell line that grows in an IL-2-dependent manner, and proliferation was measured.

(E) Same as (D) but cells were pulsed with an 11-amino-acid peptide (190-201 LLO). Results are shown from three independent experiments.

experiment (Figure 7B). Furthermore, the CFU count was significantly higher in the lungs and spleen of *Mfn2*$^{floxed;\ Cre\text{-}LysM}$ mice than in WT animals (Figure 7B).

We also examined the role of Mfn2 in LPS-induced endotoxemia. To this end, in previous assays, we determined the sub-lethal intraperitoneal dose of LPS. We then monitored mouse survival at this dose. Mice start to die at 36 h post-injection, and the survival at 4 days of *Mfn2*$^{floxed;\ Cre\text{-}LysM}$ mice was strongly reduced, reaching a significant decrease of more than 60% (Figure 7C). The serum levels of TNF-α were increased in *Mfn2*$^{floxed;\ Cre\text{-}LysM}$ mice, and this increase negatively correlated with survival (Figure 7C). In addition, 2 groups of 4 mice (WT and *Mfn2*$^{floxed;\ Cre\text{-}LysM}$) were sacrificed 48 h after LPS injection. Histopathological lesions attributable to LPS inoculation were present in both WT and *Mfn2*$^{floxed;\ Cre\text{-}LysM}$ mice; however, the lesions, particularly those in the kidney, heart (Figures S7B–S7E), lungs, and retroperitoneal and adipose tissue, tended to be more numerous and intense in the *Mfn2*$^{floxed;\ Cre\text{-}LysM}$ mice. Specifically, the necrosis of bone marrow tissue was observed only in the latter (Figures S7F and S7G). Our data demonstrate that Mfn2-deficient mice were more susceptible to LPS-induced septic shock.

These results suggest an apparent contradiction between *in vitro* and *in vivo* data concerning the LPS-dependent induction of TNF-α. However, it has been reported that the ingestion of apoptotic bodies inhibits pro-inflammatory cytokine production (Fadok et al., 1998). Indeed, this may explain the enhanced TNF-α production detected in Mfn2-deficient macrophages, which show a decrease in the phagocytosis of apoptotic bodies. Thus, we propose that Mfn2-deficient macrophages experience massive TNF-α production during endotoxin shock because the low ingestion of apoptotic bodies does not lead the cells to switch to an anti-inflammatory phenotype.

To provide further evidence of this, we incubated macrophages with apoptotic bodies for 1 h. These cells were then washed and further incubated with LPS for 18 h. Macrophages activated with LPS and apoptotic bodies showed a negative correlation between phagocytosis and TNF-α production (Figure 7D). Thus, TNF-α production was greater in Mfn2-deficient macrophages than in the WT group (Figure 7D). In contrast, under conditions in which macrophages were incubated with LPS but without apoptotic bodies, WT cells showed higher TNF-α production than Mfn2-deficient cells (Figure 7D). In these studies, the latter cells showed a decreased capacity to phagocytose apoptotic bodies (Figure S7H).

These results support a previous observation showing that phagocytosis of apoptotic bodies by LPS-treated macrophages inhibits the secretion of pro-inflammatory cytokines, such as TNF-α or IL-1β, thus inducing the switch from a pro- to anti-inflammatory phenotype (Fadok et al., 1998).

All these results indicate that Mfn2 deficiency in macrophages severely impairs the ability of the organism to fight infectious agents.

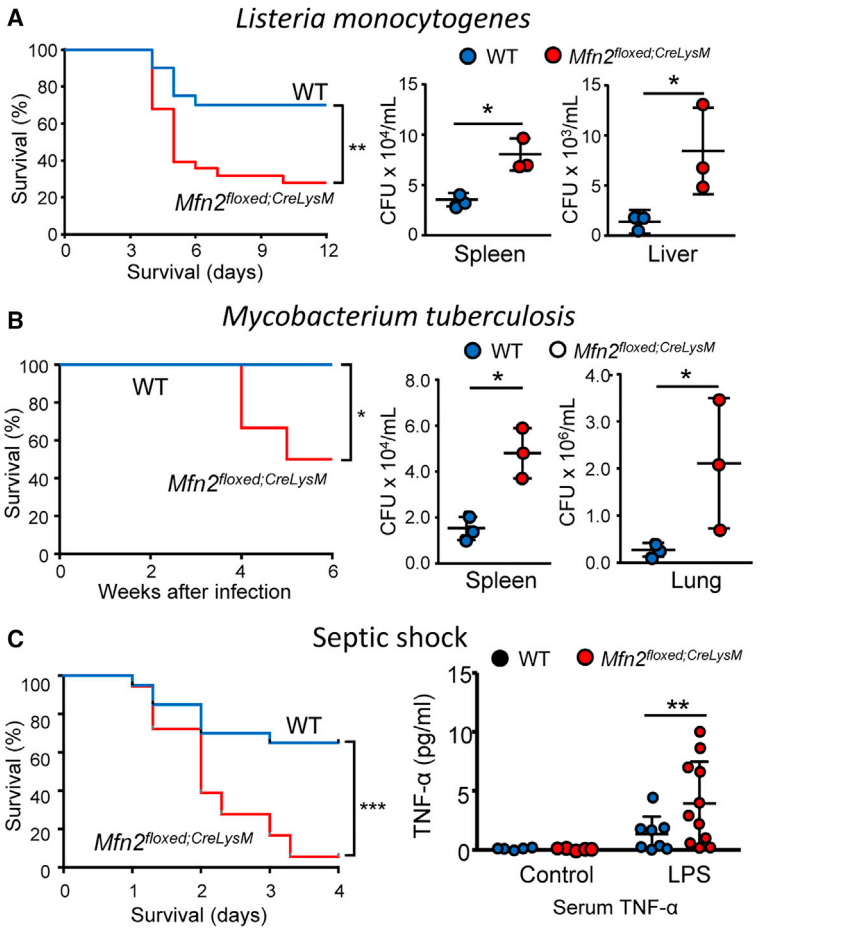

Figure 7. *Mfn2*$^{floxed;CreLysM}$ Mice Fail to be Protected from *Listeria monocytogenes*, *Mycobacterium tuberculosis*, or LPS Endotoxemia

(A) Left panel: mice were infected by intraperitoneal injection of *Listeria monocytogenes*, and survival was measured (12 mice per group in 2 independent experiments, in the figure results were pooled). Right panel: CFU count in spleen and liver lysates from 48-h infected mice (6 mice per group in 2 independent experiments).

(B) Left panel: mice infected with *Mycobacterium tuberculosis* with an aerosol, and survival was determined (12 mice per group). Right panel: CFU count in lung and spleen lysates from infected mice (3 mice per group).

(C) Left panel: mice were injected intraperitoneally with LPS, and survival was measured (10 mice per group in 2 independent experiments; in the figure, results were pooled). Right panel: mice were injected intraperitoneally with LPS and sacrificed 24 h later. TNF-α was then determined in serum (5 mice per control group and 8 WT and 11 Mfn2$^{floxed;CreLysM}$ mice treated with LPS).

(D) TNF-α secretion of BMDMs incubated *in vitro* for 1 h with media (control), apoptotic bodies, or apoptotic bodies plus LPS. Cells were then washed and incubated in media for 17 h. Supernatants were obtained, and the cytokine was measured. As a control, TNF-α secretion was determined in LPS-treated macrophages without addition of apoptotic bodies. The results are shown from three independent experiments.

See also Figure S7.

DISCUSSION

Mitochondrial fusion proteins Mfn1 and Mfn2 show key similarities but also profound differences. Both proteins are present at the outer mitochondrial membrane and show GTP binding activity. However, Mfn1 shows a higher affinity to GTP than Mfn2 (Ishihara et al., 2004). In addition, Mfn1 shows much greater GTPase activity than Mfn2 (Ishihara et al., 2004). It has recently been documented that Mfn2 but not Mfn1 has the capacity to bind phosphatidylserine (PS) *in vitro* and to promote the transfer of PS from the ER to mitochondria (Hernandez-Alvarez et al., 2019).

In mouse models, it has been clearly recognized that Mfn1 and Mfn2 exert distinct roles. Specific ablation of Mfn2 in the liver causes insulin resistance, glucose intolerance, liver disease, and ER stress (Hernandez-Alvarez et al., 2019; Sebastián et al., 2012). In contrast, Mfn1 ablation in the liver protects against insulin resistance and does not lead to ER stress (Kulkarni et al., 2016).

In addition, ablation of Mfn2 in hypothalamic pro-opiomelanocortin (POMC) neurons causes ER stress, leptin resistance, and, as a result, hyperphagia, reduced energy expenditure, and obesity (Schneeberger et al., 2013). In contrast, ablation of Mfn1 specifically in POMC neurons causes attenuated hypothalamic gene expression programs during the fast-to-fed transition, and this attenuation is linked to altered insulin secretion (Ramirez et al., 2017).

It is interesting to note that agents that induce stress, such as the TLR ligands (LPS, CPGB, or R848) induced Mfn2, but not Mfn1, in macrophages. This observation suggests that Mfn2 is a critical protein for the macrophage during stress, when large amounts of ROS are required. In keeping with this idea, it has been shown that LPS induces mitochondrial repurposing by reducing ATP synthesis and enhancing ROS production through oxidation of succinate and mitochondrial hyperpolarization (Mills et al., 2016). These metabolic alterations induce the pro-inflammatory function of macrophages.

Mfn2 is a ubiquitous protein, with particularly high expression in brain, heart, and skeletal muscle (Bach et al., 2003). The high expression of Mfn2 in macrophages, which show levels as elevated as those in brain and heart, suggest that this protein plays an important role in these cells. Indeed, Mfn2 expression levels in BMDMs were very similar to those found in peritoneal macrophages.

The absence of Mfn2 in macrophages resulted in aberrant mitochondrial morphology, including increased fragmentation and decreased mitochondrial volume. These findings support other observations in various cellular models, such as mouse embryonic fibroblasts (MEFs) (Chen et al., 2003), skeletal muscle cells and hepatocytes (Sebastián et al., 2012), and cardiac cells (Hall et al., 2016). As reported in other cell types, despite the morphological abnormalities observed in the mitochondria of macrophages, the total mitochondrial mass of these cells is not altered (Mourier et al., 2015; Papanicolaou et al., 2011).

Mfn2 controls $m\Delta\psi$ in macrophages, as described in other cellular models (Fang et al., 2016; Papanicolaou et al., 2011). This parameter is an indicator of the energization state of mitochondria, which is generated when protons are pumped from the matrix to the inner membrane space as a result of electron flow through the electron transport chain. Therefore, a low $m\Delta\psi$ can be associated with an impaired respiratory capacity, which is precisely what we observed in *Mfn2*$^{-/-}$ macrophages. Under steady-state conditions, the absence of Mfn2 did not alter mitochondrial respiration. However, although control macrophages increased their respiration under stress conditions, this was not the case for *Mfn2*$^{-/-}$ macrophages, whose mitochondrial respiration was unaltered. In the absence of Mfn2, this lack of change was probably related to the low levels of mitochondrial coenzyme Q10, which is responsible for the optimal function of the respiratory chain (Mourier et al., 2015).

Changes in the $m\Delta\psi$ and mitochondrial respiration lead to alterations in mROS production. These highly reactive molecules are generated by the leakage of electrons from the respiratory chain, resulting in a partial reduction of molecular oxygen. Therefore, increased mitochondrial respiration and $m\Delta\psi$ imply a higher flow of electrons through the electron transport chain and potentially a greater leakage of electrons, thus producing superoxide (Handy and Loscalzo, 2012). The stimulation of macrophages by pro-inflammatory activators induced a massive production of ROS, which are necessary not only to ensure the correct activation of several signaling pathways but also to kill bacteria (Tur et al., 2017; Weinberg et al., 2015; West et al., 2011b), a cellular function that is exclusive to phagocytes. Interestingly, in contrast to other cells, such as cardiomyocytes (Chen et al., 2012; Song et al., 2014), in which a lack of Mfn2 induces an increase in ROS production, in macrophages, ROS production is decreased under basal conditions and particularly when macrophages are stimulated by pro-inflammatory pathogen-associated molecular patterns (PAMP) ligands of TLR, but not by the major endogenous activator IFN-γ. This specificity is similar to the induction of Mfn2, thereby suggesting that this is a primitive system of immune stress to achieve protection against infectious agents.

Interestingly, Mfn2 is necessary to generate ROS not only during LPS activation but also under basal conditions. This observation therefore suggests that the defect in ROS production in *Mfn2*$^{-/-}$ macrophages is the result of widespread dysfunctional mitochondrial activity rather than a failure in TLR signal transduction (West et al., 2011a). This notion is supported by the observation that ROS induction with antimycin A, which directly triggers mROS at the respiratory complexes, is also dependent on Mfn2.

The disrupted ROS production in *Mfn2*$^{-/-}$ macrophages has dramatic effects on the immune response. First, we observed a reduction of LPS induction of pro-inflammatory cytokine production, which is probably associated with the decrease in ROS levels (Emre et al., 2007; Park et al., 2015). In addition, LPS-treated *Mfn2*$^{-/-}$ macrophages showed reduced p38 and ERK phosphorylation levels, probably as a result of the decreased amount of ROS. Without enough ROS, the cysteine and methionine residues from proteins in these pathways cannot be oxidized, thus potentially disrupting their activity. These observations may explain the defective sterile inflammation in *Mfn2*$^{floxed;\ Cre\text{-}LysM}$ mice.

Second, we observed that the lack of Mfn2 in macrophages was associated with an accumulation of autophagosomes, and when analyzing the autophagic flux, we found that Mfn2 was also crucial for the lysosomal degradation of autophagosomes. A similar phenotype has been described in cardiomyocytes and in skeletal muscle and the proposed underlying mechanism involved the Mfn2 recruitment of RAB7, a protein necessary for autophagosome-lysosome fusion (Sebastián et al., 2016; Zhao et al., 2012). This increase in autophagy and autophagosome accumulation may explain the alterations observed in apoptosis, phagocytosis, and protein degradation. All these factors contribute to deteriorated resistance to infections, as well as to improper antigen presentation, which are critical events for the correct activity of a healthy immune system. Importantly, our data identify Mfn2 in macrophages as an early mechanism through which the immune system responds to infection by establishing an axis TLR, mitochondria, and ROS.

Our conclusions were supported by the results of *in vivo* experimental models related to infection. The absence of Mfn2 in myeloid cells led to increased susceptibility to *L. monocytogenes* and to *M. tuberculosis,* two infections in which macrophages play a critical role. A single-nucleotide polymorphism (SNP) of *MFN2* that confers susceptibility to tuberculosis has recently been reported in humans (Qi et al., 2017), thereby supporting our observations.

Although Mfn2$^{-/-}$ macrophages incubated *in vitro* produced lower levels of TNF-α in response to LPS, *in vivo* mice lacking Mfn2 died more frequently under lethal dose 50 (LD_{50}) doses of LPS than their counterparts. This apparent contradiction can be attributed to the defect in phagocytosis associated with the

lack of Mfn2. Phagocytosis of apoptotic bodies is a critical event that switches the macrophage from a pro- to an anti-inflammatory phenotype (Fadok et al., 1998) to prevent excess destruction (Valledor et al., 2010). The early stages of endotoxin shock are characterized by massive TNF-α production, which induces tissue destruction. In WT mice, the macrophages switched to an anti-inflammatory phenotype after phagocytosis of apoptotic bodies and stopped producing TNF-α. However, Mfn2-deficient mice showed decreased phagocytosis, and although *in vitro* the production of TNF-α slowly decreased (Figure 3D), the levels of circulating TNF-α *in vivo* were increased in $Mfn2^{floxed;\ Cre\text{-}LysM}$ mice (Figure 7D). The *in vitro* experiments confirmed that, after phagocytosis of apoptotic bodies, the phenotype of LPS-activated macrophages switched to produce lower amounts of TNF-α (Figure 7D), thereby confirming previous observations (Byrne and Reen, 2002; Fadok et al., 1998; Lucas et al., 2003). Given that $Mfn2^{-/-}$ macrophages showed lower levels of phagocytosis, they continued to produce TNF-α. This suggests an *in vivo* role of phagocytosis in the switch of macrophages to an anti-inflammatory phenotype. However, we cannot exclude other possibilities to explain the apparent contradiction between the *in vivo* production of TNF-α and the *in vitro* results.

Mfn1 also plays a role in mitochondrial fusion and shares 80% similarity to Mfn2 (Chen and Chan, 2004), but contrary to Mfn2, production of mROS was not modified in relation to the controls or even after LPS stimulation. Using the conditional KO mouse of Mfn1, we suggested that the anomalies caused by Mfn2 were related to the lack of ROS.

Finally, it was recently shown that the uptake of multiple apoptotic bodies by macrophages requires dynamin-related protein 1 (Drp1), a molecule that mediates mitochondrial fission (Wang et al., 2017). This observation, together with our results, emphasizes the critical role of the mitochondria dynamics of macrophages in the homeostasis of the immune system.

STAR★METHODS

Detailed methods are provided in the online version of this paper and include the following:

- KEY RESOURCES TABLE
- RESOURCE AVAILABILITY
  - Lead Contact
  - Materials Availability
  - Data and Code Availability
- EXPERIMENTAL MODEL AND SUBJECT DETAILS
  - Bacterial strains
  - Cell lines
  - Primary cell cultures
- EXPERIMENTAL MODEL AND SUBJECT DETAILS
- METHOD DETAILS
  - RNA extraction, reverse-PCR, and qPCR
  - Mitochondrial DNA quantification
  - Telomere measurement
  - Western blot protein analysis
  - Extracellular and intracellular staining and flow cytometry
  - Mitochondrial mass and membrane potential
  - Mitochondrial fluorescence microscopy
  - Mitochondrial respiration and glycolytic metabolism
  - ROS measurements
  - Arginase activity assay
  - ATP measurement
  - Determination of TNF-α, IL-6, nitrites and cellular proliferation
  - Cell cycle analysis
  - Phagocytosis assays
  - Bactericidal activity
  - *In vitro* Listeria monocytogenes infection
  - Phagocytosis of apoptotic bodies
  - Apoptosis
  - Antigen presentation assay
  - Mouse DNFB ear inflammation assay
  - Mouse Listeria monocytogenes challenge
  - Mouse Mycobacterium tuberculosis challenge
  - Mouse LPS endotoxemia challenge
- QUANTIFICATION AND STATISTICAL ANALYSIS

SUPPLEMENTAL INFORMATION

Supplemental Information can be found online at https://doi.org/10.1016/j.celrep.2020.108079.

ACKNOWLEDGMENTS

This work was supported by Ministerio de Economía y Competitividad (MINECO) grants SAF2014-52887-R and BFU2017-85353 (J.L. and A.C.), MINECO grant SAF2013-40987R (A.Z.), Generalitat de Catalunya grant 2014SGR48 (A.Z.), the Spanish Biomedical Research Centre in Diabetes and Associated Metabolic Disorders (CIBERDEM) (A.Z.), Programa de Cooperación Interregiones IV-B Europa Suroccidental (INTERREG IVB-SUDOE-FEDER) (DIOMED, SOE1/P1/E178) (A.Z.), and INFLAMES (PIE-14/00045, El Instituto de Salud Carlos III [ISCIII], Spain). A.Z. is a recipient of a Catalan Institution for Research and Advanced Studies (ICREA) "Academia" award (Generalitat de Catalunya). The Institute for Research in Biomedicine (IRB Barcelona) is recipient of the Severo Ochoa Award of Excellence from MINECO. J.T. and S.P.-L. were supported by Formación del Profesorado Universitario grants AP2012-02327 and AP2010-5396, respectively, from the Ministerio de Educación, Cultura y Deporte. We thank Dr. Emil R. Unanue, from the Washington University School of Medicine, St. Louis, Missouri, for reagents and advice in antigen presentation assays. We thank Dr. Neus Prats for tissue evaluation of mouse autopsies (Histopathology Core Facility, IRB Barcelona) and Nuria Elias for technical work.

AUTHOR CONTRIBUTIONS

J.T. and J.P.M. conceived and performed the experiments and wrote the manuscript. S.P.-L., T.V., E.A.M., and M.H.-A. performed experiments. P.-J.C. provided expertise and feedback. A.Z., J.L., and A.C. conceived the experiments, wrote the manuscript, and secured funding.

DECLARATION OF INTERESTS

The authors declare no competing interests.

Received: July 27, 2018
Revised: July 2, 2020
Accepted: August 5, 2020
Published: August 25, 2020

REFERENCES

Bach, D., Pich, S., Soriano, F.X., Vega, N., Baumgartner, B., Oriola, J., Daugaard, J.R., Lloberas, J., Camps, M., Zierath, J.R., et al. (2003). Mitofusin-2 determines mitochondrial network architecture and mitochondrial metabolism. A novel regulatory mechanism altered in obesity. J. Biol. Chem. *278*, 17190–17197.

Bach, D., Naon, D., Pich, S., Soriano, F.X., Vega, N., Rieusset, J., Laville, M., Guillet, C., Boirie, Y., Wallberg-Henriksson, H., et al. (2005). Expression of Mfn2, the Charcot-Marie-Tooth neuropathy type 2A gene, in human skeletal muscle: effects of type 2 diabetes, obesity, weight loss, and the regulatory role of tumor necrosis factor alpha and interleukin-6. Diabetes *54*, 2685–2693.

Bettigole, S.E., and Glimcher, L.H. (2015). Endoplasmic reticulum stress in immunity. Annu. Rev. Immunol. *33*, 107–138.

Biswas, S.K., and Mantovani, A. (2012). Orchestration of metabolism by macrophages. Cell Metab. *15*, 432–437.

Bodgan, C. (2001). Nitric oxide and the immune response. Nat Immunol. *2*, 907–916.

Bombelli, F., Stojkovic, T., Dubourg, O., Echaniz-Laguna, A., Tardieu, S., Larcher, K., Amati-Bonneau, P., Latour, P., Vignal, O., Cazeneuve, C., et al. (2014). Charcot-Marie-Tooth disease type 2A: from typical to rare phenotypic and genotypic features. JAMA Neurol. *71*, 1036–1042.

Bonilla, D.L., Bhattacharya, A., Sha, Y., Xu, Y., Xiang, Q., Kan, A., Jagannath, C., Komatsu, M., and Eissa, N.T. (2013). Autophagy regulates phagocytosis by modulating the expression of scavenger receptors. Immunity *39*, 537–547.

Bonneville, M., Chavagnac, C., Vocanson, M., Rozieres, A., Benetiere, J., Pernet, I., Denis, A., Nicolas, J.F., and Hennino, A. (2007). Skin contact irritation conditions the development and severity of allergic contact dermatitis. J. Invest. Dermatol. *127*, 1430–1435.

Bustin, S.A., Benes, V., Garson, J.A., Hellemans, J., Huggett, J., Kubista, M., Mueller, R., Nolan, T., Pfaffl, M.W., Shipley, G.L., et al. (2009). The MIQE guidelines: minimum information for publication of quantitative real-time PCR experiments. Clin. Chem. *55*, 611–622.

Byrne, A., and Reen, D.J. (2002). Lipopolysaccharide induces rapid production of IL-10 by monocytes in the presence of apoptotic neutrophils. J. Immunol. *168*, 1968–1977.

Callicott, R.J., and Womack, J.E. (2006). Real-time PCR assay for measurement of mouse telomeres. Comp. Med. *56*, 17–22.

Cardona, P.J., Gordillo, S., Díaz, J., Tapia, G., Amat, I., Pallarés, A., Vilaplana, C., Ariza, A., and Ausina, V. (2003). Widespread bronchogenic dissemination makes DBA/2 mice more susceptible than C57BL/6 mice to experimental aerosol infection with Mycobacterium tuberculosis. Infect. Immun. *71*, 5845–5854.

Carrero, J.A., Vivanco-Cid, H., and Unanue, E.R. (2012). Listeriolysin o is strongly immunogenic independently of its cytotoxic activity. PLoS One *7*, e32310.

Casals, C., Barrachina, M., Serra, M., Lloberas, J., and Celada, A. (2007). Lipopolysaccharide up-regulates MHC class II expression on dendritic cells through an AP-1 enhancer without affecting the levels of CIITA. J. Immunol. *178*, 6307–6315.

Celada, A., Gray, P.W., Rinderknecht, E., and Schreiber, R.D. (1984). Evidence for a gamma-interferon receptor that regulates macrophage tumoricidal activity. J. Exp. Med. *160*, 55–74.

Chen, H., and Chan, D.C. (2004). Mitochondrial dynamics in mammals. Curr. Top. Dev. Biol. *59*, 119–144.

Chen, H., Detmer, S.A., Ewald, A.J., Griffin, E.E., Fraser, S.E., and Chan, D.C. (2003). Mitofusins Mfn1 and Mfn2 coordinately regulate mitochondrial fusion and are essential for embryonic development. J. Cell Biol. *160*, 189–200.

Chen, H., McCaffery, J.M., and Chan, D.C. (2007). Mitochondrial fusion protects against neurodegeneration in the cerebellum. Cell *130*, 548–562.

Chen, Y., Csordás, G., Jowdy, C., Schneider, T.G., Csordás, N., Wang, W., Liu, Y., Kohlhaas, M., Meiser, M., Bergem, S., et al. (2012). Mitofusin 2-containing mitochondrial-reticular microdomains direct rapid cardiomyocyte bioenergetic responses via interorganelle Ca(2+) crosstalk. Circ. Res. *111*, 863–875.

Classen, A., Lloberas, J., and Celada, A. (2009). Macrophage activation: classical versus alternative. Methods Mol. Biol. *531*, 29–43.

Clausen, B.E., Burkhardt, C., Reith, W., Renkawitz, R., and Förster, I. (1999). Conditional gene targeting in macrophages and granulocytes using LysMcre mice. Transgenic Res. *8*, 265–277.

de Brito, O.M., and Scorrano, L. (2008a). Mitofusin 2 tethers endoplasmic reticulum to mitochondria. Nature *456*, 605–610.

de Brito, O.M., and Scorrano, L. (2008b). Mitofusin 2: a mitochondria-shaping protein with signaling roles beyond fusion. Antioxid. Redox Signal. *10*, 621–633.

Ding, Y., Gao, H., Zhao, L., Wang, X., and Zheng, M. (2015). Mitofusin 2-deficiency suppresses cell proliferation through disturbance of autophagy. PLoS One *10*, e0121328.

Emre, Y., Hurtaud, C., Nübel, T., Criscuolo, F., Ricquier, D., and Cassard-Doulcier, A.M. (2007). Mitochondria contribute to LPS-induced MAPK activation via uncoupling protein UCP2 in macrophages. Biochem. J. *402*, 271–278.

Fadok, V.A., Bratton, D.L., Konowal, A., Freed, P.W., Westcott, J.Y., and Henson, P.M. (1998). Macrophages that have ingested apoptotic cells in vitro inhibit proinflammatory cytokine production through autocrine/paracrine mechanisms involving TGF-beta, PGE2, and PAF. J. Clin. Invest. *101*, 890–898.

Fang, D., Yan, S., Yu, Q., Chen, D., and Yan, S.S. (2016). Mfn2 is Required for Mitochondrial Development and Synapse Formation in Human Induced Pluripotent Stem Cells/hiPSC Derived Cortical Neurons. Sci. Rep. *6*, 31462.

Formentini, L., Santacatterina, F., Núñez de Arenas, C., Stamatakis, K., López-Martínez, D., Logan, A., Fresno, M., Smits, R., Murphy, M.P., and Cuezva, J.M. (2017). Mitochondrial ROS Production Protects the Intestine from Inflammation through Functional M2 Macrophage Polarization. Cell Rep. *19*, 1202–1213.

Gijbels, M.J., and de Winther, M.P. (2011). Autopsy and histological analysis of the transgenic mouse. Methods Mol. Biol. *693*, 75–87.

Hall, A.R., Burke, N., Dongworth, R.K., Kalkhoran, S.B., Dyson, A., Vicencio, J.M., Dorn, G.W., II, Yellon, D.M., and Hausenloy, D.J. (2016). Hearts deficient in both Mfn1 and Mfn2 are protected against acute myocardial infarction. Cell Death Dis. *7*, e2238.

Handy, D.E., and Loscalzo, J. (2012). Redox regulation of mitochondrial function. Antioxid. Redox Signal. *16*, 1323–1367.

Harvey, C.J., Thimmulappa, R.K., Sethi, S., Kong, X., Yarmus, L., Brown, R.H., Feller-Kopman, D., Wise, R., and Biswal, S. (2011). Targeting Nrf2 signaling improves bacterial clearance by alveolar macrophages in patients with COPD and in a mouse model. Sci. Transl. Med. *3*, 78ra32.

Hellemans, J., Mortier, G., De Paepe, A., Speleman, F., and Vandesompele, J. (2007). qBase relative quantification framework and software for management and automated analysis of real-time quantitative PCR data. Genome Biol. *8*, R19.

Hernandez-Alvarez, M.I., Sebastian, D., Vives, S., Ivanova, S., Bartoccioni, P., Kakimoto, P., Plana, N., Veiga, S.R., Hernandez, V., Vasconcelos, N., et al. (2019). Deficient Endoplasmic Reticulum-Mitochondrial Phosphatidylserine Transfer Causes Liver Disease. Cell *177*, 881–895.e817.

Hotamisligil, G.S. (2010). Endoplasmic reticulum stress and the inflammatory basis of metabolic disease. Cell *140*, 900–917.

Hurley, J.H., and Young, L.N. (2017). Mechanisms of Autophagy Initiation. Annu. Rev. Biochem. *86*, 225–244.

Ichinohe, T., Yamazaki, T., Koshiba, T., and Yanagi, Y. (2013). Mitochondrial protein mitofusin 2 is required for NLRP3 inflammasome activation after RNA virus infection. Proc. Natl. Acad. Sci. USA *110*, 17963–17968.

Ishihara, N., Eura, Y., and Mihara, K. (2004). Mitofusin 1 and 2 play distinct roles in mitochondrial fusion reactions via GTPase activity. J. Cell Sci. *117*, 6535–6546.

Kulkarni, S.S., Joffraud, M., Boutant, M., Ratajczak, J., Gao, A.W., Maclachlan, C., Hernandez-Alvarez, M.I., Raymond, F., Metairon, S., Descombes, P., et al. (2016). Mfn1 Deficiency in the Liver Protects Against Diet-Induced Insulin Resistance and Enhances the Hypoglycemic Effect of Metformin. Diabetes *65*, 3552–3560.

Liesa, M., and Shirihai, O.S. (2013). Mitochondrial dynamics in the regulation of nutrient utilization and energy expenditure. Cell Metab. *17*, 491–506.

Lloberas, J., Valverde-Estrella, L., Tur, J., Vico, T., and Celada, A. (2016). Mitogen-Activated Protein Kinases and Mitogen Kinase Phosphatase 1: A Critical Interplay in Macrophage Biology. Front. Mol. Biosci. *3*, 28.

Lucas, M., Stuart, L.M., Savill, J., and Lacy-Hulbert, A. (2003). Apoptotic cells and innate immune stimuli combine to regulate macrophage cytokine secretion. J. Immunol. *171*, 2610–2615.

Mariño, G., Niso-Santano, M., Baehrecke, E.H., and Kroemer, G. (2014). Self-consumption: the interplay of autophagy and apoptosis. Nat. Rev. Mol. Cell Biol. *15*, 81–94.

Mills, E.L., Kelly, B., Logan, A., Costa, A.S.H., Varma, M., Bryant, C.E., Tourlomousis, P., Dabritz, J.H.M., Gottlieb, E., Latorre, I., et al. (2016). Succinate Dehydrogenase Supports Metabolic Repurposing of Mitochondria to Drive Inflammatory Macrophages. Cell *167*, 457–470.e413.

Mourier, A., Motori, E., Brandt, T., Lagouge, M., Atanassov, I., Galinier, A., Rappl, G., Brodesser, S., Hultenby, K., Dieterich, C., and Larsson, N.G. (2015). Mitofusin 2 is required to maintain mitochondrial coenzyme Q levels. J. Cell Biol. *208*, 429–442.

Muñoz, J.P., Ivanova, S., Sánchez-Wandelmer, J., Martínez-Cristóbal, P., Noguera, E., Sancho, A., Díaz-Ramos, A., Hernández-Alvarez, M.I., Sebastián, D., Mauvezin, C., et al. (2013). Mfn2 modulates the UPR and mitochondrial function via repression of PERK. EMBO J. *32*, 2348–2361.

Ngoh, G.A., Papanicolaou, K.N., and Walsh, K. (2012). Loss of mitofusin 2 promotes endoplasmic reticulum stress. J. Biol. Chem. *287*, 20321–20332.

Nogueras, M.M., Merino, S., Aguilar, A., Benedi, V.J., and Tomás, J.M. (2000). Cloning, sequencing, and role in serum susceptibility of porin II from mesophilic Aeromonas hydrophila. Infect. Immun. *68*, 1849–1854.

Orsi, R.H., Bergholz, T.M., Wiedmann, M., and Boor, K.J. (2015). The Listeria monocytogenes strain 10403S BioCyc database. Database (Oxford) *2015*, bav027.

Papanicolaou, K.N., Khairallah, R.J., Ngoh, G.A., Chikando, A., Luptak, I., O'Shea, K.M., Riley, D.D., Lugus, J.J., Colucci, W.S., Lederer, W.J., et al. (2011). Mitofusin-2 maintains mitochondrial structure and contributes to stress-induced permeability transition in cardiac myocytes. Mol. Cell. Biol. *31*, 1309–1328.

Park, J., Min, J.S., Kim, B., Chae, U.B., Yun, J.W., Choi, M.S., Kong, I.K., Chang, K.T., and Lee, D.S. (2015). Mitochondrial ROS govern the LPS-induced pro-inflammatory response in microglia cells by regulating MAPK and NF-κB pathways. Neurosci. Lett. *584*, 191–196.

Peiser, L., Gough, P.J., Kodama, T., and Gordon, S. (2000). Macrophage class A scavenger receptor-mediated phagocytosis of Escherichia coli: role of cell heterogeneity, microbial strain, and culture conditions in vitro. Infect. Immun. *68*, 1953–1963.

Peng, C., Rao, W., Zhang, L., Wang, K., Hui, H., Wang, L., Su, N., Luo, P., Hao, Y.L., Tu, Y., et al. (2015). Mitofusin 2 ameliorates hypoxia-induced apoptosis via mitochondrial function and signaling pathways. Int. J. Biochem. Cell Biol. *69*, 29–40.

Pereira-Lopes, S., Tur, J., Calatayud-Subias, J.A., Lloberas, J., Stracker, T.H., and Celada, A. (2015). NBS1 is required for macrophage homeostasis and functional activity in mice. Blood *126*, 2502–2510.

Poon, I.K., Lucas, C.D., Rossi, A.G., and Ravichandran, K.S. (2014). Apoptotic cell clearance: basic biology and therapeutic potential. Nat. Rev. Immunol. *14*, 166–180.

Portnoy, D.A., Auerbuch, V., and Glomski, I.J. (2002). The cell biology of Listeria monocytogenes infection: the intersection of bacterial pathogenesis and cell-mediated immunity. J. Cell Biol. *158*, 409–414.

Qi, H., Zhang, Y.B., Sun, L., Chen, C., Xu, B., Xu, F., Liu, J.W., Liu, J.C., Chen, C., Jiao, W.W., et al. (2017). Discovery of susceptibility loci associated with tuberculosis in Han Chinese. Hum. Mol. Genet. *26*, 4752–4763.

Ramirez, S., Gomez-Valades, A.G., Schneeberger, M., Varela, L., Haddad-Tovolli, R., Altirriba, J., Noguera, E., Drougard, A., Flores-Martinez, A., Imbernon, M., et al. (2017). Mitochondrial Dynamics Mediated by Mitofusin 1 Is Required for POMC Neuron Glucose-Sensing and Insulin Release Control. Cell Metab. *25*, 1390–1399.e1396.

Schindelin, J., Arganda-Carreras, I., Frise, E., Kaynig, V., Longair, M., Pietzsch, T., Preibisch, S., Rueden, C., Saalfeld, S., Schmid, B., et al. (2012). Fiji: an open-source platform for biological-image analysis. Nat. Methods *9*, 676–682.

Schneeberger, M., Dietrich, M.O., Sebastián, D., Imbernón, M., Castaño, C., Garcia, A., Esteban, Y., Gonzalez-Franquesa, A., Rodríguez, I.C., Bortolozzi, A., et al. (2013). Mitofusin 2 in POMC neurons connects ER stress with leptin resistance and energy imbalance. Cell *155*, 172–187.

Sebastián, C., Herrero, C., Serra, M., Lloberas, J., Blasco, M.A., and Celada, A. (2009). Telomere shortening and oxidative stress in aged macrophages results in impaired STAT5a phosphorylation. J. Immunol. *183*, 2356–2364.

Sebastián, D., Hernández-Alvarez, M.I., Segalés, J., Sorianello, E., Muñoz, J.P., Sala, D., Waget, A., Liesa, M., Paz, J.C., Gopalacharyulu, P., et al. (2012). Mitofusin 2 (Mfn2) links mitochondrial and endoplasmic reticulum function with insulin signaling and is essential for normal glucose homeostasis. Proc. Natl. Acad. Sci. USA *109*, 5523–5528.

Sebastián, D., Sorianello, E., Segalés, J., Irazoki, A., Ruiz-Bonilla, V., Sala, D., Planet, E., Berenguer-Llergo, A., Muñoz, J.P., Sánchez-Feutrie, M., et al. (2016). Mfn2 deficiency links age-related sarcopenia and impaired autophagy to activation of an adaptive mitophagy pathway. EMBO J. *35*, 1677–1693.

Sebastián, D., Palacín, M., and Zorzano, A. (2017). Mitochondrial Dynamics: Coupling Mitochondrial Fitness with Healthy Aging. Trends Mol. Med. *23*, 201–215.

Song, M., and Dorn, G.W., 2nd. (2015). Mitoconfusion: noncanonical functioning of dynamism factors in static mitochondria of the heart. Cell Metab. *21*, 195–205.

Song, M., Chen, Y., Gong, G., Murphy, E., Rabinovitch, P.S., and Dorn, G.W., II. (2014). Super-suppression of mitochondrial reactive oxygen species signaling impairs compensatory autophagy in primary mitophagic cardiomyopathy. Circ. Res. *115*, 348–353.

Soriano, F.X., Liesa, M., Bach, D., Chan, D.C., Palacín, M., and Zorzano, A. (2006). Evidence for a mitochondrial regulatory pathway defined by peroxisome proliferator-activated receptor-gamma coactivator-1 alpha, estrogen-related receptor-alpha, and mitofusin 2. Diabetes *55*, 1783–1791.

Tur, J., Vico, T., Lloberas, J., Zorzano, A., and Celada, A. (2017). Macrophages and Mitochondria: A Critical Interplay Between Metabolism, Signaling, and the Functional Activity. Adv. Immunol. *133*, 1–36.

Twig, G., Hyde, B., and Shirihai, O.S. (2008). Mitochondrial fusion, fission and autophagy as a quality control axis: the bioenergetic view. Biochim. Biophys. Acta *1777*, 1092–1097.

Valledor, A.F., Comalada, M., Santamaría-Babi, L.F., Lloberas, J., and Celada, A. (2010). Macrophage proinflammatory activation and deactivation: a question of balance. Adv. Immunol. *108*, 1–20.

Verhoeven, K., Claeys, K.G., Züchner, S., Schröder, J.M., Weis, J., Ceuterick, C., Jordanova, A., Nelis, E., De Vriendt, E., Van Hul, M., et al. (2006). MFN2 mutation distribution and genotype/phenotype correlation in Charcot-Marie-Tooth type 2. Brain *129*, 2093–2102.

Wang, Y., Subramanian, M., Yurdagul, A., Jr., Barbosa-Lorenzi, V.C., Cai, B., de Juan-Sanz, J., Ryan, T.A., Nomura, M., Maxfield, F.R., and Tabas, I. (2017). Mitochondrial Fission Promotes the Continued Clearance of Apoptotic Cells by Macrophages. Cell *171*, 331–345.e322.

Weinberg, S.E., Sena, L.A., and Chandel, N.S. (2015). Mitochondria in the regulation of innate and adaptive immunity. Immunity *42*, 406–417.

West, A.P., Brodsky, I.E., Rahner, C., Woo, D.K., Erdjument-Bromage, H., Tempst, P., Walsh, M.C., Choi, Y., Shadel, G.S., and Ghosh, S. (2011a). TLR

signalling augments macrophage bactericidal activity through mitochondrial ROS. Nature *472*, 476–480.

West, A.P., Shadel, G.S., and Ghosh, S. (2011b). Mitochondria in innate immune responses. Nat. Rev. Immunol. *11*, 389–402.

Youle, R.J., and van der Bliek, A.M. (2012). Mitochondrial fission, fusion, and stress. Science *337*, 1062–1065.

Zhang, W., Shu, C., Li, Q., Li, M., and Li, X. (2015). Adiponectin affects vascular smooth muscle cell proliferation and apoptosis through modulation of the mitofusin-2-mediated Ras-Raf-Erk1/2 signaling pathway. Mol. Med. Rep. *12*, 4703–4707.

Zhao, T., Huang, X., Han, L., Wang, X., Cheng, H., Zhao, Y., Chen, Q., Chen, J., Cheng, H., Xiao, R., and Zheng, M. (2012). Central role of mitofusin 2 in autophagosome-lysosome fusion in cardiomyocytes. J. Biol. Chem. *287*, 23615–23625.

Zorzano, A., Liesa, M., Sebastián, D., Segalés, J., and Palacín, M. (2010). Mitochondrial fusion proteins: dual regulators of morphology and metabolism. Semin. Cell Dev. Biol. *21*, 566–574.

Zorzano, A., Hernandez-Alvarez, M.I., Sebastian, D., and Munoz, J.P. (2015). Mitofusin 2 as a driver that controls energy metabolism and insulin signaling. Antioxid. Redox Signal. *22*, 1020–1031.

Züchner, S., Mersiyanova, I.V., Muglia, M., Bissar-Tadmouri, N., Rochelle, J., Dadali, E.L., Zappia, M., Nelis, E., Patitucci, A., Senderek, J., et al. (2004). Mutations in the mitochondrial GTPase mitofusin 2 cause Charcot-Marie-Tooth neuropathy type 2A. Nat. Genet. *36*, 449–451.

STAR★METHODS

KEY RESOURCES TABLE

REAGENT or RESOURCE	SOURCE	IDENTIFIER
Antibodies		
Goat anti-mouse (HRP)	Abcam	Cat# ab6789; RRID: AB_955439
Goat anti-rabbit (HRP)	Jackson	Cat# 111-035-003;RRID: AB_2313567
Isotype IgG2a κ	ThermoFisher	Cat# 56-4321; RRID: AB_494018
Isotype IgG2b κ	Becton and Dickinson	Cat# 553989; RRID: AB_10049479
Isotype IgM κ	Becton and Dickinson	Cat# 553942 RRID: AB_479631
Mouse anti-JNK1/2	Santa Cruz	Cat# SC-137019; RRID: AB_2140722
Mouse anti-JNK1/2 (pT183/pY185)	BD Biosciences	Cat# 612541; RRID: AB_399838
Mouse anti-β-actin	Sigma Aldrich	Cat# A-5441; RRID: AB_476744
Mouse anti-alpha-tubulin	Sigma Aldrich	Cat# B-5-1-2 T5168; RRID: AB_477579
Rabbit anti-ERK1/2	Cell signaling	Cat# 4695S; RRID: AB_390779
Rabbit anti-ERK1/2 (pT202/pY204)	Cell signaling	Cat# 4370S; RRID: AB_2315112
Rabbit anti-LC3	Sigma Aldrich	Cat# L8918; RRID: AB_1079382
Rabbit anti-MKP1	Upstate	Cat#07-535; RRID: AB_310697
Rabbit anti-NF-κB (pSer536)	Cell signaling	Cat# 4887; RRID: AB_561198
Rabbit anti-p38	Cell signaling	Cat# 9212S; RRID: AB_330713
Rabbit anti-p38 (pT180/pY182)	Cell signaling	Cat# 9211S; RRID: AB_331641
Rabbit anti-STAT6 (pY641)	Cell signaling	Cat# 9361S; RRID: AB_331595
Rabbit anti-NRF2	Cell signalling	Cat# mAb #12721; RRID: AB_2715528
Rat anti- CD115, IgG2a κ	ThermoFisher	Cat# 12-1152-82; RRID: AB_465808
Rat anti-CD11b, IgG2b κ	BD Pharmigen	Cat# 553310; RRID: AB_394774
Rat anti-CD16/32	BD Pharmigen	Cat# 553141; RRID: AB_394656
Rat anti-CD3, IgG2b κ	Biolegend	Cat# 100203: RRID: AB_312660
Rat anti-CD45, IgG2b κ	ThermoFisher	Cat# 25-0451-82; RRID: AB_2734986
Rat anti-CD45R, IgG2a κ	ThermoFisher	Cat# RM2629; RRID: AB_10373822
Rat anti-F4/80, IgG2a κ	ThermoFisher	Cat# 17-4801-80; RRID: AB_2784647
Rat anti-Ly6C, IgM κ	BD Pharmigen	Cat# 553104; RRID: AB_394628
Rat anti-MHC-II I-A/I-E, IgG2a κ	BD Pharmigen	Cat# 553623; RRID: AB_394958
Bacterial Strains		
Aeromonas hydrophila (serovar O:34)	Nogueras et al., 2000	N/A
Listeria monocytogenes (strain10403S)	Orsi et al., 2015	N/A
Mycobacterium tuberculosis (strain H37Rv)	Cardona et al., 2003	N/A
Chemicals, Peptides, and Recombinant Proteins		
Dulbecco's modified Eagle's medium (DMEM)	Cultek	Cat# 12-604F
CellStripper	Corning	Cat# CLS3008
Heat-Inactivated Fetal Bovine Serum	GIBCO	Cat# 10082147
Roswell Park Memorial Institute (RPMI) 1640	Sigma-Aldrich	Cat# R8758
Brain Heart Infusion Agar	Sigma-Aldrich	Cat# 70138
LB Broth with agar	Sigma-Aldrich	Cat# L2897
1x PBS	Corning	Cat# 21-022-CV
Penicillin/Streptomycin	Sigma-Aldrich	Cat# P0781
Murine recombinant interleukin (IL)-2	R&D Systems	Cat# 402-ML

(*Continued on next page*)

Continued

REAGENT or RESOURCE	SOURCE	IDENTIFIER
Murine recombinant interferon gamma (IFN-γ)	R&D Systems	Cat# 485-ML
Murine recombinant interleukin (IL)-4	R&D Systems	Cat# 404-ML
Murine Macrophage Colony Stimulating Factor (M-CSF)	Peprotech	Cat# 315-02
Murine Granulocyte Macrophage Colony Stimulating Factor (GM-CSF)	Peprotech	Cat# 315-03
CpG B oligodeoxynucleotides (ODN)	Invivogen	Cat# ODN 1668
R848	Invivogen	Cat# tlrl-r848
Lipopolysaccharide (LPS)	Sigma-Aldrich	Cat# L3129
Paraformaldehyde	Sigma-Aldrich	Cat# 158127
Triton-X10	Sigma-Aldrich	Cat# X100
Ethanol	AppliChem PanReac	Cat# A3678
Propidium iodide	Sigma-Aldrich	Cat# P-4170
RNase A	Sigma-Aldrich	Cat# R-6513
2′7′-dichlorofluorescin diacetate (DCF-DA)	Sigma Aldrich	Cat# D6883
Antimycin A	Sigma Aldrich	Cat# A8674
n-acetyl cysteine (NAC)	Sigma Aldrich	Cat# A8199
MitoSox red	Molecular Probes	Cat# M36008
MitoTracker green	Invitrogen	Cat# M7514
MitoTracker deep red	Invitrogen	Cat# M22426
Calcein	ThermoFisher	Cat# C1430
Hoechst 33342	ThermoFishe	Cat# 62249
(5(6)-Carboxyfluorescein N-hydroxysuccinimidyl ester) (CSFE)	Sigma Aldrich	Cat# 762040
Cytochalasin D	Sigma-Aldrich	Cat# C8273
8-well μ-slide plates	Ibidi	Cat# 80826
Protease inhibitors	Sigma Aldrich	Cat# P8465
PVDF Gel TransferStacks	Life Technologies	Cat# B24002
ECL	Amersham Biosciences	Cat# RPN2108
Bradford Protein Assay	Bio-Rad laboratories	Cat#
X-ray films	FujiFilm	Cat# SuperRX
Blotting grade blocker	Bio Rad	Cat# 1706404EDU
Tween 20	Sigma-Aldrich	Cat# P9416
L-arginine	Sigma-Aldrich	Cat# A5006
MnCl2	Innogenetics	Cat# 28305
α–isonitrosopropiophenone (α-ISPP)	Sigma-Aldrich	Cat# 220094
Carbonil cyanide 3-chlorophenylhydrazone	Sigma-Aldrich	Cat# C2759
Rotenone	Sigma-Aldrich	Cat# R8875
Oligomycin A	Sigma-Aldrich	Cat# 75351
Optimum cutting temperature (O.C.T.)	Tissue Tek	Cat# 4583
Critical Commercial Assays		
Annexin V-FITC Apoptosis Detection Kit	Abcam	Cat# ab14085
DNeasy Blood and Tissue Kit	QIAGEN	Cat# 69506
Griess Reagent Kit	Promega	Cat# G2930
Moloney Murine Leukemia Virus Reverse Transcriptase	Promega	Cat# M1302
Mouse TNF-α ELISA Ready-SET-go!	eBioscience	Cat# 88-7324
Mouse IL-6 ELISA	Invitrogen	Cat# 88-7064

(*Continued on next page*)

Continued

REAGENT or RESOURCE	SOURCE	IDENTIFIER
OxyBlot Kit	Millipore	Cat# S7150
ReliaPrep RNA Miniprep Systems	Promega	Cat# Z6010
SYBR Green Master Mix	Applied Biosystems	Cat# 4309155
SYBR® Green RT-PCR Reagents Kit	Applied Biosystems	Cat# 4306736
TMRE-Mitochondrial potential assay kit	Abcam	Cat# ab113852
Experimental Models: Cell Lines		
Mouse: Apoptotic bodies	This paper	N/A
Mouse: Bone Marrow-Derived Macrophage cells	This paper	N/A
Mouse: $CD4^+$ T cell hybridomas against the 190-201 segment of listeriolysin O (LLO)	Carrero et al., 2012	N/A
Mouse: Elicited Peritoneal Macrophage cells	This paper	N/A
Mouse: IL-2-dependent CTLL-2	ATCC	ATCC TIB-214
Mouse: L-929 Fibroblast cells	ATCC	ATCC CCL-1
Mouse: Thymocytes	This paper	N/A
Experimental Models: Organisms/Strains		
Mouse: *Mfn2*$^{flox/flox}$ C57BL/6J	Chen et al., 2007	N/A
Mouse: *Mfn1*$^{flox/flox}$ C57BL/6J	Chen et al., 2007	N/A
Mouse: *CreLysM* C57BL/6J	Clausen et al., 1999	N/A
Mouse: *Mfn2*$^{flox\ Cre-}$ C57BL/6J	This paper	N/A
Mouse: *Mfn2*$^{floxed;CreLysM}$	This paper	N/A
Oligonucleotides		
See Table S1 for qPCR primer probes	N/A	N/A
Software and Algorithms		
Biogazelle Qbase+ software	Biogazelle	https://www.qbaseplus.com/
FlowJo Version 10	FlowJo	https://www.flowjo.com/solutions/flowjo/downloads
Imaris software Version 9.6	Bitplane	https://imaris.oxinst.com
Open-source image analysis software	Fiji	https://imagej.net/Fiji
Prism Version 5.0	GraphPad Software Inc.	https://www.graphpad.com/

RESOURCE AVAILABILITY

Lead Contact

Further information and requests for resources and reagents should be directed to and will be fulfilled by the Lead Contact, Antonio Celada (acelada@ub.edu).

Materials Availability

This study did not generate new unique reagents.

Data and Code Availability

This study did not generate any unique datasets or code.

EXPERIMENTAL MODEL AND SUBJECT DETAILS

Bacterial strains

Aeromonas hydrophila (serovar O:34) with a pWIL plasmid-containing eGFP was kindly provided by Dr. Susana Merino (University of Barcelona, Spain), and was grown at 37°C in LB-agar plates. *Listeria monocytogenes* (strain10403S) was a kind gift from Dr. Carlos Ardavín (National Center for Biotechnology/CSIC, Madrid, Spain), and was grown at 37°C in brain-heart infusion agar plates.

Cell lines

L-929 (mouse fibroblasts) cells were maintained in Dulbecco's modified Eagle's medium (DMEM) supplemented with 10% (vol/vol) heat-inactivated fetal bovine serum (HI-FBS), 10 U/mL penicillin and 100 mg/mL streptomycin. Cells were cultured in a humidified CO2 incubator at 37°C. L-929 cells were originally derived from normal adipose tissue from a 100-day-old male C3H/An mouse.

$CD4^+$ T cell hybridomas against the 190-201 segment of listeriolysin O (LLO) has been described (Carrero et al., 2012). The hybridomas were maintained in DMEM+10% FBS. The IL-2-dependent CTLL-2 cell line was maintained in RPMI 1640, 2 mM Glutamine, 10 U/ml recombinant IL-2 and10% FBS.

Primary cell cultures

Bone marrow-derived macrophages (BMDMs) were generated from 6- to 12-week-old mice as described (Celada et al., 1984). Briefly, epiphyses from femora and tibiae were removed, and these bones were flushed with pre-warmed DMEM to extract the bone marrow. Bone marrow cells were cultured in Petri dishes with DMEM-containing 20% (vol/vol) heat inactivated FBS, 30% L-cell-conditioned media as M-CSF source, 100 U/mL penicillin, and 100 μg/mL streptomycin. Cells were incubated at 37°C in a humidified 5% CO_2 atmosphere. Macrophages loosely adhere to the Petri dishes and were harvested with cold PBS without causing cell death. A homogeneous population of adherent macrophages was obtained after seven days of culture (> 98% CD11b and F4/80 positive cells). Unless stated otherwise, BMDMs were left for 16 h in medium without M-CSF to allow synchronization of cell cycles prior to stimulation.

Murine peritoneal macrophages were obtained from a peritoneal lavage with sterile PBS as described (Celada et al., 1984). Briefly, 10 mL of ice-cold PBS was injected intraperitoneally into mice previously sacrificed by cervical dislocation. PBS from the peritoneal cavity was then recovered, and cells were pelleted down and cultured in plastic dishes for 3 h at 37°C in a humidified 5% CO_2 atmosphere with DMEM containing 10% FBS. Non-adherent cells were then discarded thus leaving the adherent population of peritoneal macrophages.

Unless specified otherwise, the concentrations of cytokines, growth factors, and PAMPs used to activate macrophages were the following: IFN-γ, IL-4, LPS, M-CSF and GM-CSF 10 ng/ml; CpGB 100 nM/ml; and R848 1 μg/ml. LPS was purchased from Sigma-Aldrich (L3129, Lipopolysaccharides from *Escherichia coli* O127:B8). In previous experiments, the results obtained with the commercial LPS were compared with highly purified LPS from *Salmonella abortus* equi, provided by Dr. C. Galanos (Max Planck Institute, Freiburg, Germany) (Casals et al., 2007). No differences were found between the two.

EXPERIMENTAL MODEL AND SUBJECT DETAILS

All animal work was conducted following the guidelines established by the Animal Research Committee of the Catalan Government (number 9158). Mice were socially housed under a 12 h light/dark cycle with *ad libitum* access to water and food. They were randomly assigned to experimental groups. $Mfn2^{floxed;CreLysM}$ mice were obtained by crossing $Mfn2^{floxp/floxp}$ and $Mfn1^{floxp/floxp}$ mice (kindly provided by Dr. David Chan, through the Mutant Mouse Regional Resource Center) and a mouse strain expressing Cre recombinase under the control of myeloid-specific promoter lysozyme M (CreLysM) (a generous gift from Dr. Ángel Nebreda, IRB Barcelona). Both colonies were generated in a C57BL/6JRj background. $Mfn2^{floxed;CreLysM}$ descendants and the corresponding WT mice ($Mfn2^{Flox\ Cre-}$) from the same background were maintained in the SPF facility at the Barcelona Science Park. In all procedures, female mice at the age of 8 to 10 weeks old were used.

METHOD DETAILS

RNA extraction, reverse-PCR, and qPCR

Total RNA was extracted, purified, and treated with DNase using the ReliaPrep RNA system kit, as recommended by the manufacturer. 400 ng of RNA was retrotranscribed to cDNA using the Moloney murine leukemia virus (MMLV) reverse transcriptase RNase H Minus, following the manufacturer's specifications. Quantitative PCR (qPCR) was performed using SYBR Green Master Mix, as recommended by the manufacturer. Non-retrotranscribed RNA samples were used as negative controls for each gene. When signal was detected in these negative controls (< 32 Ct), the primer pairs used were discarded and replaced with alternative ones for the same gene. Furthermore, the amplification efficiency for each pair of primers was calculated by making a standard curve of serially diluted cDNA samples. Only the pairs of primers with an amplification efficiency of 100 ± 10% were used. The list of primers can be found in Table S1.

Data were analyzed by the ΔΔCt method (Bustin et al., 2009) using Biogazelle Qbase+ software. Gene expression was normalized to three reference genes (i.e., housekeeping genes): *Hprt1*, *L14*, and *Sdha* (unless otherwise specified). The stability of these reference genes was determined by checking that their geNorm M value was lower than 0.5 (Hellemans et al., 2007).

Mitochondrial DNA quantification

Total DNA from 10^6 BMDMs cultured in 12-well plates in DMEM+10%FBS for 16 h was isolated using the DNeasy Blood and Tissue Kit and following the manufacturer's instructions. DNA concentration and purity was quantified in a NanoDrop ND-1000 system (Thermo Scientific). qPCR with this DNA was performed as described before. The number of copies of mitochondrial DNA

(mDNA) was calculated by measuring the expression of two mitochondrial-encoded genes, namely Cytochrome *c* oxidase I and Nadh dehydrogenase II, and normalizing them by the expression of two single-copy nuclear-encoded genes, β-2 microglobulin and PE-CAM1. The relative expression of the ribosomal subunit 18S, a multicopy nuclear gene, was used as control.

Telomere measurement

Telomere length was measured as described (Callicott and Womack, 2006). Briefly, genomic DNA was extracted with the DNeasy Blood and Tissue Kit and qPCR was performed as described. Telomere length was calculated by measuring the relative number of telomere copies to two single-copy nuclear genes (T/S ratio, β-2 microglobulin and PE-CAM1).

Western blot protein analysis

To obtain total protein lysates, BMDMs (at least 10^6 cells) were washed in cold PBS and lysed with TGH-NaCl (1% Triton X-100, 10% glycerol, 50 mM HEPES, and 250 mM NaCl) plus protease inhibitors, as indicated (Pereira-Lopes et al., 2015). Lysates were centrifuged to remove cellular debris. The protein concentration was determined using the Bradford Protein Assay. Total protein lysates (50 μg) were separated by SDS-PAGE and transferred to polyvinylidene difluoride (PVDF) membranes using the iBlot2 system (Thermo Fisher) and following the manufacturer's instructions. Membranes were blocked for 1 h at room temperature in blocking buffer (5% dry milk in TBS-0.1% Tween 20) and then incubated with primary antibody in blocking buffer for 16 h at 4°C. The membranes were then washed three times x 5 min with TBS-Tween and incubated for 1 h at room temperature with the corresponding horseradish peroxidase (HRP)-conjugated secondary antibody diluted 1:1000 in blocking buffer. After washing as before, ECL detection was performed, and membranes were exposed to X-ray films. When necessary, band intensity was quantified using the open-source image analysis software Fiji (Schindelin et al., 2012). Anti-ERK1/2, anti-ERK1/2 (pT202/pY204), anti-MKP1, anti-STAT6 (pY641), anti-p38 and p38 (pT180/Y182) were used at a dilution of 1:1,000; anti-JNK1/2, anti-JNK1/2 (pT183/Y185) and anti-LC3 at 1:500 dilution; and anti-β-actin at 1:10000 dilution.

Extracellular and intracellular staining and flow cytometry

For extracellular marker staining, BMDMs were collected, resuspended in staining buffer (5% FBS in PBS), and seeded in 96-well plates at 4°C with 5 mM EDTA. Fc gamma receptors were blocked using an anti-CD16/CD32 antibody for 15 min at 4°C. Labeling was performed by incubating the cells with the correspondent antibody mix for 30 min at 4°C. An isotype for each antibody was used as control.

For intracellular NF-κB staining, BMDMs were collected, resuspended in staining buffer, and transferred to 96-well plates (10^5 cells/well). They were then fixed in 4% paraformaldehyde for 15 min. After that, they were permeabilized with 0.2% Triton-X10 for 5 min. FcγRs were then blocked and the cells were stained. The antibody used was Phospho-NF-κB subunit p65 diluted 1:50. In this case, DAPI gating was not used to discriminate dead cells.

After staining, samples were acquired in a Gallios Flow Cytometer (Beckman coulter). Unless otherwise specified, the following gating strategy was followed: first, macrophages (or leukocytes when specified) were selected on the basis of their forward (FS-A) and side scatter (SS-A). Singlets were then selected using FS-A and the signal peak height (FS-H) parameters. Finally, dead cells were discriminated by DAPI staining. Data were analyzed with FlowJo 10.

Mitochondrial mass and membrane potential

To stain mitochondria and quantify mitochondrial mass, BMDMs were stained with MitoTracker Green following the manufacturer's instructions. Mean fluorescence intensity (MFI) was used to measure mitochondrial mass. Mitochondrial membrane potential was assessed with TMRE-Mitochondrial Membrane Potential Assay Kit and following the manufacturer's instructions.

Mitochondrial fluorescence microscopy

10^5 BMDMs were seeded in 8-well μ-slide plates. Cells were washed with cold PBS and incubated with MitoTracker Deep Red, as recommended by the manufacturer. Microscopy images were obtained in a Leica SP2 spectral confocal microscope (AOBS system), maintaining 37°C and 5% CO_2 for the duration of the experiment. Confocal images were recorded every 0.5 μm in the z-plane to record the whole cellular volume. Five images with at least 20 cells were captured for each condition. Images were analyzed using Imaris software. For each cell, the number of isolated components (a measure of the degree of mitochondrial fragmentation) and the average volume per mitochondrion was measured.

Mitochondrial respiration and glycolytic metabolism

An XF24 analyzer (Seahorse Biosciences) was used to measure BMDM mitochondrial function in real time. Macrophages were seeded into XF24 cell culture plates at a density of $2x10^5$ cells/well and left for 16 h in medium without M-CSF in a 37°C-humidified incubator with 5% CO2. Medium was replaced by un-buffered XF assay medium with 5 mM glucose and 2 mM L-glutamine and then equilibrated in a non-CO_2 incubator for 1 h. The oxygen consumption ratio (OCR) and extracellular acidification rate (ECAR: a measure of glycolysis) were analyzed by sequentially adding drugs that modify the activity of the electron transport chain (ETC). Oligomycin was used at a concentration of 625 nM to target ATP synthase, and ATP coupling was measured. Cyanide m-chlorophenyl hydrazone (CCCP) used at 1.25 μM targets the inner mitochondrial membrane and measures maximal respiration; rotenone used

at 1 μM targets Complex I and measures OCR inhibition, and antimycin A used at 1 μM targets Complex III and measures OCR inhibition.

The following respiration parameters were calculated: a) Basal respiration: energy demand under baseline conditions (calculated as the third OCR measurement under basal conditions); b) ATP coupling: respiration to meet ATP production (obtained by adding oligomycin); c) Maximal respiration: maximum rate of respiration a cell can achieve (obtained by adding CCCP); d) Spare respiratory capacity: capacity of the cell to respond to increased energy demands (calculated as the increase in % from basal to maximal respiration); and e) Non-mitochondrial respiration: oxygen consumed by non-mitochondrial sources (obtained by adding antimycin A and rotenone). The concentrations of substrates and inhibitors used were based on prior experiments conducted for the optimization of the titration protocols.

ROS measurements

Mitochondrial superoxide production (mROS) was measured by incubating BMDMs with MitoSox red, following the manufacturer's instructions. Hydrogen peroxide (total cellular ROS) was measured by staining cells with 50 μM 2′7′-dichlorofluorescin diacetate (DCF-DA) (Sigma Aldrich), as described (Pereira-Lopes et al., 2015). When indicated, 5 μM antimycin A or 10 mM n-acetyl cysteine (NAC) was used to modulate ROS production. Protein oxidation was detected with the OxyBlot Kit.

Arginase activity assay

Arginase activity was measured as described (Classen et al., 2009). Briefly, 10^5 BMDMs were cultured in 96-well plates and stimulated with IL-4 for 24 h. After washing, cells were lysed in 0.1%Triton. Arginase activity was measured in the lysates by adding L-arginine and $MnCl_2$, and finally, optical density at 540 nm was read after reaction with α-isonitrosopropiophenone (α-ISPP).

ATP measurement

10^6 BMDMs were cultured in 6-well plates for 16 h in DMEM+10%FBS. The cells were then washed in cold PBS and lysed in 100 mM Tris-HCl+4mM EDTA (pH 7.75) by thermal shock (quick-freeze in liquid nitrogen and an immediate thaw in a 37°C water bath buffer). ATP from lysates was measured using the ATP-determination kit, following the manufacturer's protocol. Total protein from lysates was also measured using the Bradford Protein Assay. The results were expressed as amount of ATP normalized by protein concentration.

Determination of TNF-α, IL-6, nitrites and cellular proliferation

BMDMs (10^5 cells) were plated in 96-well plates. They were then stimulated with the indicated reagents for the indicated times or left untreated. Supernatant was collected and diluted 1/8. TNF-α was determined using the Mouse TNF-α ELISA Ready-SET-go! kit (eBioscience) and IL-6 using the mouse IL-6 ELISA kit (Invitrogen) following the manufacturer's instructions. Nitrites were measured using the Griess Reagent Kit (Promega) and cellular proliferation using the Cell Proliferation ELISA BrdU kit (Roche).

Cell cycle analysis

BMDMs (10^6) were cultured in DMEM+10%FBS in 12-well plates for 16 h. They were then left unstimulated or treated as specified for 24 h and then fixed with 95% ethanol. Next, cells were incubated with propidium iodide (PI) and RNase A. Cell cycle distributions were analyzed on the basis of IP staining (G1, S, and G2).

Phagocytosis assays

BMDMs (10^6 cells) were cultured in 12-well plates in DMEM+10%FBS without antibiotics for 16 h. They were then infected with the GFP-expressing *Aeromonas hydrophila* (serovar O:34) at a multiplicity of infection (MOI) of 25. To this end, 100 μL of exponentially growing bacterial suspension was added to the macrophages and immediately centrifuged. Cells were then incubated in a 37°C 5% CO_2 incubator for the indicated periods. After that, phagocytosis was stopped by washing cells five times with 5 mM EDTA in PBS. eGFP fluorescence inside the cells was quantified by flow cytometry in a Gallios cytometer.

A phagocytosis assay was also performed using pHrodo red *S. aureus* BioParticles (Molecular probes) and pHrodo green *E. coli* BioParticles (Molecular probes) and following the manufacturer's instructions. In this case, 10^5 macrophages were cultured in a 96-well dark-bottom plate in DMEM+10%FBS for 16 h. Bioparticles (1 mg/ml) were then added, and the cells were cultured for the indicated times. pHRhodo fluorescence was quantified in a plate fluorimeter. As control, phagocytosis was measured in BMDMs treated with cytochalascin D (2 μg/ml).

Bactericidal activity

BMDMs (10^6 cells) were infected at MOI 25 with *Aeromonas hydrophila,* and a phagocytosis assay was performed for 60 min, as above. Alternatively, 60 min after infection, cells were washed three times with PBS and then incubated for 1 h with 300 μg/mL of gentamycin in DMEM+10%FBS to eliminate non-phagocytosed bacteria. Medium was then removed, and cells were washed three times with PBS. They were then lysed with 0.02%Triton X-100. Lysates were serially diluted, cultured in LB plates, and left to grow for 24 to 48 h. Colony-forming units (CFUs) were then counted.

In vitro Listeria monocytogenes infection

BMDMs (10^6 cells) were cultured in antibiotic-free DMEM+10%FBS in 12-well plates for 16 h. They were then infected at MOI 5 with exponentially growing *Listeria monocytogenes* (strain10403S). To eliminate non-phagocytosed bacteria, after 30 min of incubation medium was replaced by fresh medium comprising 5 μg/ml gentamycin in DMEM+10%FBS. RNA was extracted after 6 h of incubation, as explained before.

Phagocytosis of apoptotic bodies

Apoptotic bodies were obtained by incubating mice thymocytes with 30 μM etoposide for 16 h. After washing, apoptotic cells were stained with 5(6)-Carboxyfluorescein N-hydroxysuccinimidyl ester (CFSE) and added to a 10^6 BMDM culture in a proportion of 10:1 (Apoptotic bodies:BMDM). After 1 h of incubation, non-phagocytosed apoptotic cells were washed out, and macrophages were analyzed by flow cytometry. Incubation with 2 μg/ml cytochalascin D prior to phagocytosis was used as negative control.

Apoptosis

Apoptotis was determined by incubating BMDMs with the Annexin V-FITC Apoptosis Detection Kit, following the manufacturer's instructions. Live (double negative), necrotic (DAPI positive), early (Annexin-V positive), and late apoptotic (double positive) cell populations were detected by flow cytometry.

Antigen presentation assay

Antigen presentation was performed as described (Carrero et al., 2012). Briefly, BMDMs (10^5 cells) were incubated in 96-well plates with the indicated dilutions of antigen (listeriolysin O (LLO) or the 190-201 peptide of LLO), and then co-cultured in a 1:2 proportion with $CD4^+$ T cell hybridomas specific for that antigen. In the case of antigen presentation, the hybridomas release IL-2. After 24 h, supernatant was transferred to tubes and subjected to several freeze-thaw cycles to eliminate cells. Then supernatants were incubated with CTLL-2 cells, a line that proliferates in an IL-2-dependent manner. The proliferation of CTLL-2 cells was measured by pulsing them with ^3H-thymidine (0.5 μCi/plate) for 8 h and then counting disintegration in a β-counter. A positive control with recombinant IL-2 and a negative one with medium alone were used.

Mouse DNFB ear inflammation assay

2,4-dinitrofenolbenzene (DNFB) was diluted 1% in acetone. Female mice were anesthetized with isoflurane, and 10 μL of 1%DNFB was homogeneously applied to the whole extension of one ear. Vehicle alone (acetone) was applied to the other ear as a control (Pereira-Lopes et al., 2015). At the times indicated, mice were euthanized, and a punch of the same radius was taken in both treated and control ears to measure inflammation. Ear punches were weighed and then each one was used for both RNA extraction and histology. For histology, ear punches were fixed in 4% paraformaldehyde for 24 h and then embedded in paraffin. Ear sections were stained with hematoxylin and eosin. Images were collected with a Nikon E800 microscope, and ear thickness measurements were calculated with Fiji software (Schindelin et al., 2012).

Mouse Listeria monocytogenes challenge

Listeria monocytogenes (strain10403S) was kindly provided by Professor Carlos Ardavín (National Center for Biotechnology/CSIC, Madrid, Spain). $2x10^4$ CFU/Kg of exponentially growing *Listeria* were diluted in 5 mL of sterile PBS and injected intraperitoneally into WT and *Mfn2*$^{floxed;CreLysM}$ female mice between 8 and 12 weeks old. Survival, weight, and clinical symptoms were monitored twice a day. The experiment was stopped when all the surviving mice started to recover weight (day 12 post-infection). Moribund and surviving mice were humanely euthanized following the guidelines of the Animal Research Committee.

In additionally, a group of three mice of each genotype were separated from the others. These mice were sacrificed at day 2 post-infection, and spleen and liver were mechanically lysed, passed through a nylon strainer, serially diluted, and seeded in brain-heart media plates to quantify CFUs.

Mouse Mycobacterium tuberculosis challenge

For this experiment, female mice were shipped to the "Unitat de Tuberculosis Experimental de l'Hospital Germans Trias i Pujol," Badalona, Spain, where they were kept under controlled conditions in a P3 high-security facility. Animals were infected with a low-dose aerosol (100 CFU/mice) of *Mycobacterium tuberculosis* (strain H37Rv) (Cardona et al., 2003), and survival was monitored for six weeks. In addition, at week 3 post-infection, three mice from each group were sacrificed, and lungs and spleen lysates were seeded to count CFUs.

Mouse LPS endotoxemia challenge

Mice were injected intraperitoneally with a sublethal dose of LPS (15 mg kg^{-1}) in a volume of 500 μl that was diluted in saline. Survival after LPS challenge was assessed every 12 h for three days. All surviving mice were killed at the end of the fourth day. In addition, at 24 h post-infection, mice from each group were sacrificed, and blood was obtained by cardiac puncture. Also 4 WT and *Mfn2*$^{floxed;CreLysM}$ were sacrificed 48 h after LPS injection. Liver, retroperitoneal adipose tissue, brown and white adipose tissue, adrenal gland, brain, heart, spleen, lung, salivary gland, submandibular lymph node, kidney, stomach, large intestine, pancreas, mesentery, striated

muscle and bone marrow were removed and embedded in OCT solution. Cryosections of 10 μm were stained with hematoxylin and eosin, following standard protocols (Gijbels and de Winther, 2011). The samples were evaluated by the Histopathology Facility of the Institute of Research in Biomedicine, Barcelona, Spain.

QUANTIFICATION AND STATISTICAL ANALYSIS

Data were analyzed using the non-parametric Mann-Whitney U test or the unpaired Student's t test, as indicated in each figure legend. When two or more variables were compared, a two-way ANOVA test followed by a Bonferroni correction was used, as indicated in the figure legends. Survival curves were compared using the Mantel-Cox (log-rank) test. Center, dispersion, and n are defined in each figure legend. For all analyses, significance was set at $p < 0.05$. Statistical analyses were performed using GraphPad Prism 6.0 software.

Cell Reports, Volume *32*

Supplemental Information

Mitofusin 2 in Macrophages Links Mitochondrial ROS Production, Cytokine Release, Phagocytosis, Autophagy, and Bactericidal Activity

Juan Tur, Selma Pereira-Lopes, Tania Vico, Eros A. Marín, Juan P. Muñoz, Maribel Hernández-Alvarez, Pere-Joan Cardona, Antonio Zorzano, Jorge Lloberas, and Antonio Celada

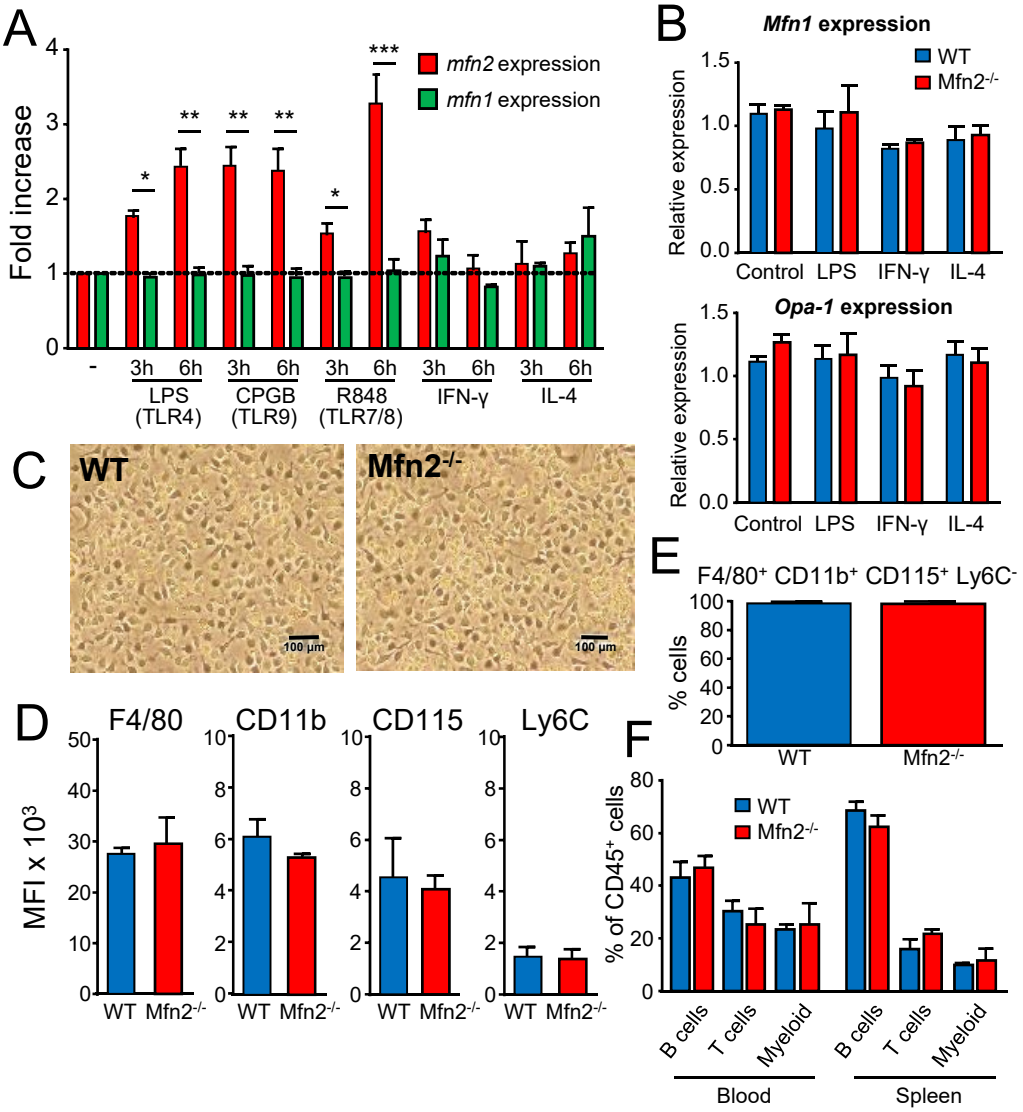

Figure S1. **Characterization of *Mfn2* in macrophages**. **(A)** *Mfn2* but not *Mfn1* is induced upon TLR stimulation. BMDM were treated with LPS (10ng/ml), CPGB (10ng/ml), R848 (10ng/ml), IFN-γ (10ng/ml) or IL-4(10ng/ml) for 24 h. The expression of *Mfn2* and *Mfn1* was measured by qPCR and the relative amount was shown as fold increase in relation to their expression in non-stimulated BMDM. **(B)** In *Mfn2*$^{-/-}$ macrophages, the expression of *Mfn1* or *Opa1* is not affected. The treatments are as indicated in (A). **(C)** Macrophage differentiation is not affected by Mfn2 deficiency. Optic microscopy images of BMDM cultures at day 7 of differentiation. Scale bar represents 100µm. Similar results were found in three independent experiments. **(D)** Mean fluorescence intensity (MFI) of different surface markers in BMDM. **(E)** Percent of cells positive for F4/80, CD11b, and CD115, and negative for Ly6C. Positive and negative gates have been established using isotypes of the correspondent antibodies. **(F)** Percent of B220^{+} cells (B cells), CD3^{+} cells (T cells), and CD11b^{+} cells (myeloid cells) relative to the whole leukocyte population (CD45^{+} cells) in spleen and blood. Results in (**C**) are representative images of at least three independent experiments. The rest of results are shown as mean ± SD from three independent experiments compared using two-way ANOVA: (*p<0.05, **p<0.01, ***p<0.001). Related to Figure 1.

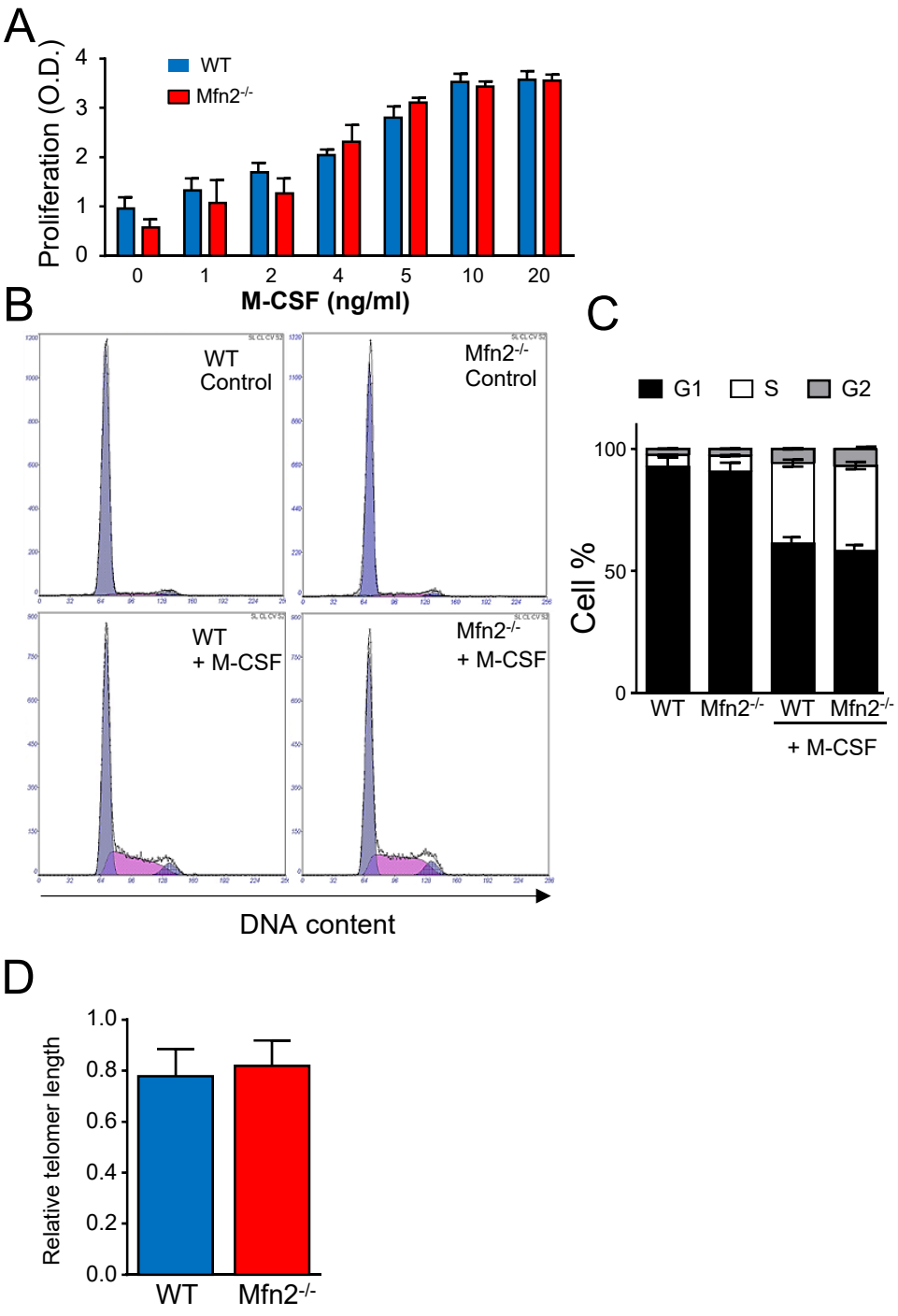

Figure S2. **Mfn2 has no effect on macrophage proliferation or senescence**. **(A)**. M-CSF-dependent proliferation was measured in control and *Mfn2*$^{-/-}$ BMDM incubated for 24h with the indicated concentrations of the growth factor. **(B and C)** Cell cycle distributions of control and M-CSF stimulated macrophages (10ng/ml for 24h). Histograms of B are representative of three independent experiments. **(D)** Relative telomere length of WT and *Mfn2*$^{-/-}$ macrophages determined by qPCR. In A, C and D results are shown as mean ± SD from three independent experiments compared using two-way ANOVA without differences. Related to Figure 1.

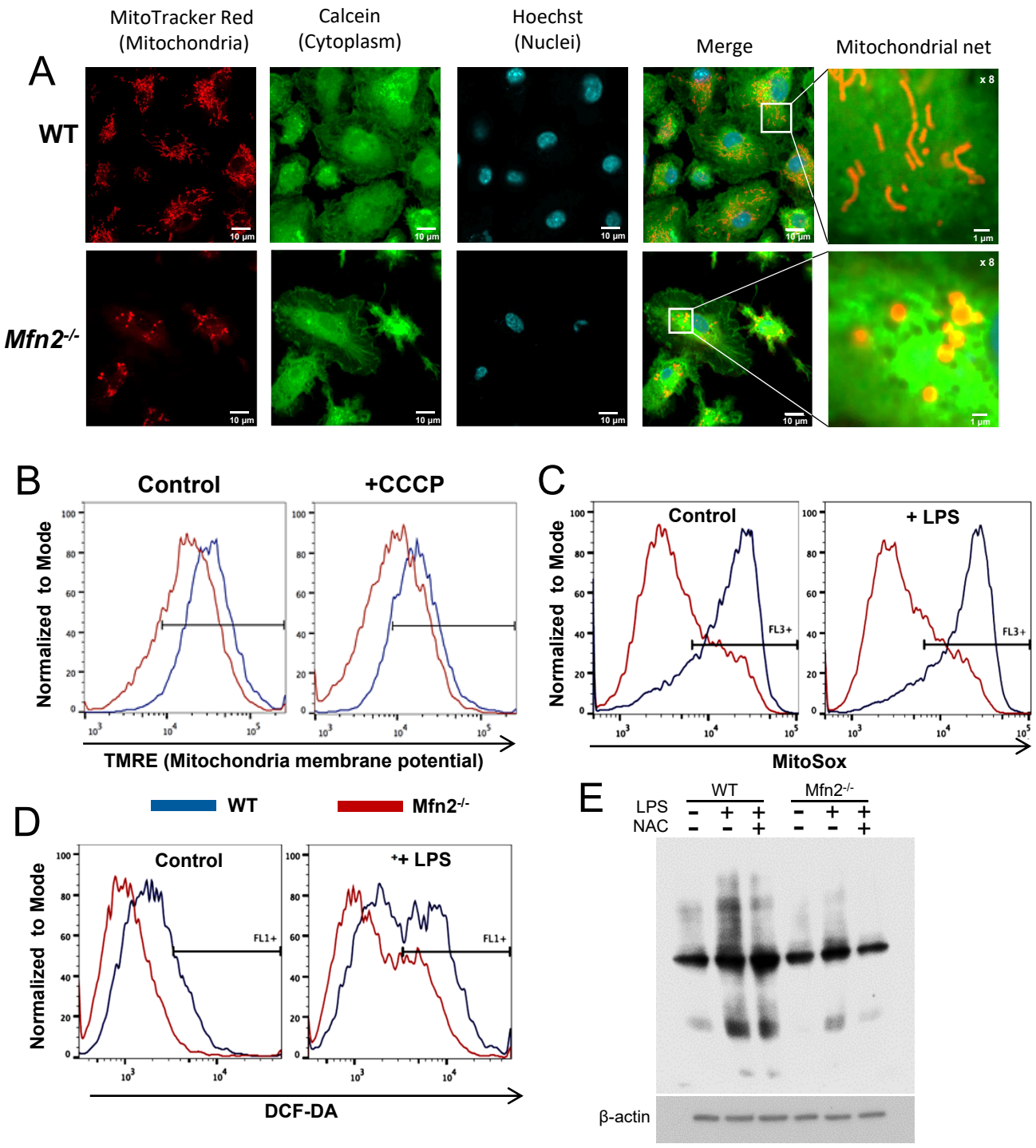

Figure S3. **Mfn2 is essential to mitochondrial integrity, function, and ROS production. (A)** Macrophage mitochondria were stained with Mitotracker MitoTracker Deep Red (mitochondria), Calcein (cytoplasm) and Hoechst (nuclei) and observed by confocal fluorescence microscopy. Zooms of Z-stacks from images. Photography are representative of five independent experiments. Scale bar represents 10µm with the exception of the amplification x8 panels (1µm) **(B)** To measure mitochondrial potential (mΔΨ) flow cytometry with TMRE staining was used. As negative control, the proton uncoupler CCCP was used. **(C)** Representative image of mROS measurement by MitoSox staining. Cells were treated with LPS (10ng/ml) for 1h. **(D)** Representative image of total cellular ROS measurement by DCF-DA staining. **(E)** Protein oxidation was detected with the OxyBlot™ Kit. 2µg of protein was used. Cells were incubated with LPS or LPS+NAC for 6h. Similar results were obtained in two other independent experiments. Related to Figure 1 and 2

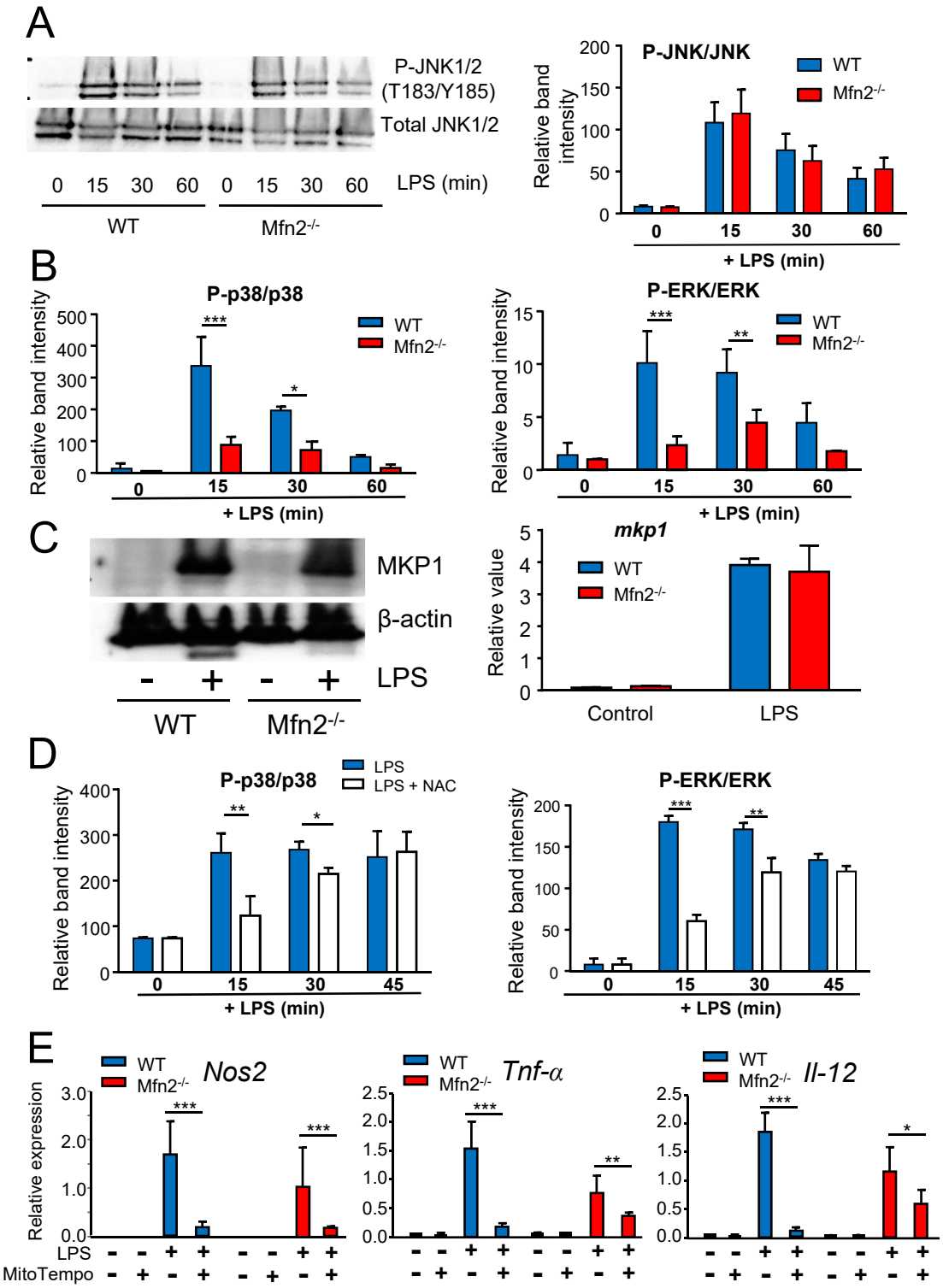

Figure S4. **Mfn2 promotes p38 and Erk activation in response to LPS. (A)** Cells were incubated with LPS (10ng/ml) for the indicated times and phosphorylation of JNK was measured by western blot. A representative blot is shown of three independent experiments and band intensity quantification is shown. **(B)** Band intensity quantification of Figure 3A in relation to the non-phosphorylated form. **(C)** WT and Mfn2$^{-/-}$ macrophages were treated with or without LPS (10ng/ml) for 1h. *mkp1* mRNA expression was determined by qPCR and the protein by Western blot which figure is representative of two independent experiments. **(D)** Band intensity quantification of Figure 3G in relation to the non-phosphorylated form. **(E)** Relative mRNA expression of *Nos2*, *Tnf-α* and *Il-12* in basal conditions after 3h of LPS stimulation with or without previous treatment with Mito Tempo (50μM). All the other graphs are shown as mean ± SD from three independent experiments compared using two-way ANOVA: *p<0.05, **p<0.01, ***p<0.001. Related to Figure 3.

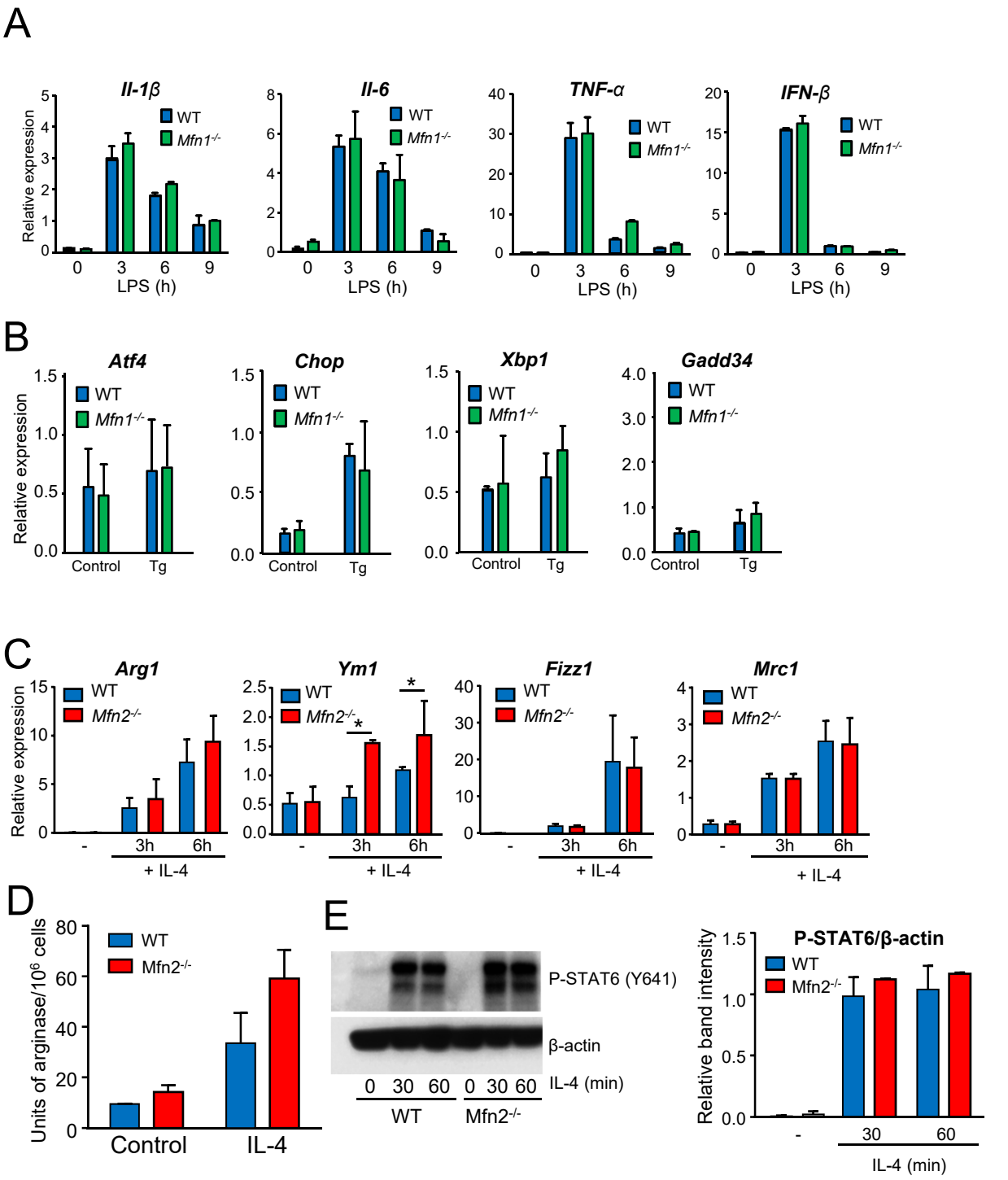

Figure S5. **The lack of Mfn1 do not alter the anti-inflammatory macrophage activation or ER stress responses**. **(A)** Control and *Mfn1*$^{-/-}$ macrophages were treated with LPS (10 ng/ml) for the indicated times, then the gene expression was determined by qPCR. **(B)** Control and *Mfn1*$^{-/-}$ macrophages were treated with Thapsigargin (Tg) (3μM) for 24h, then the gene expression was determined by qPCR. **(C)** Macrophages were treated with IL-4 (10ng/ml) for the indicated times, then the gene expression was determined by qPCR. **(D)** Macrophages were treated with IL-4 for 24h and arginase activity was determined. Arginase activity represented as units of enzyme per million of BMDMs. **(E)** Western blot of whole protein extracts from IL4 stimulated BMDMs. Band intensity of P-STAT6 relative to β-actin. Western blot in D is representative of three independent experiments. All the other results are shown as mean ± SD from three independent experiments compared using two-way ANOVA: *p<0.05 . Related to Figure 3.

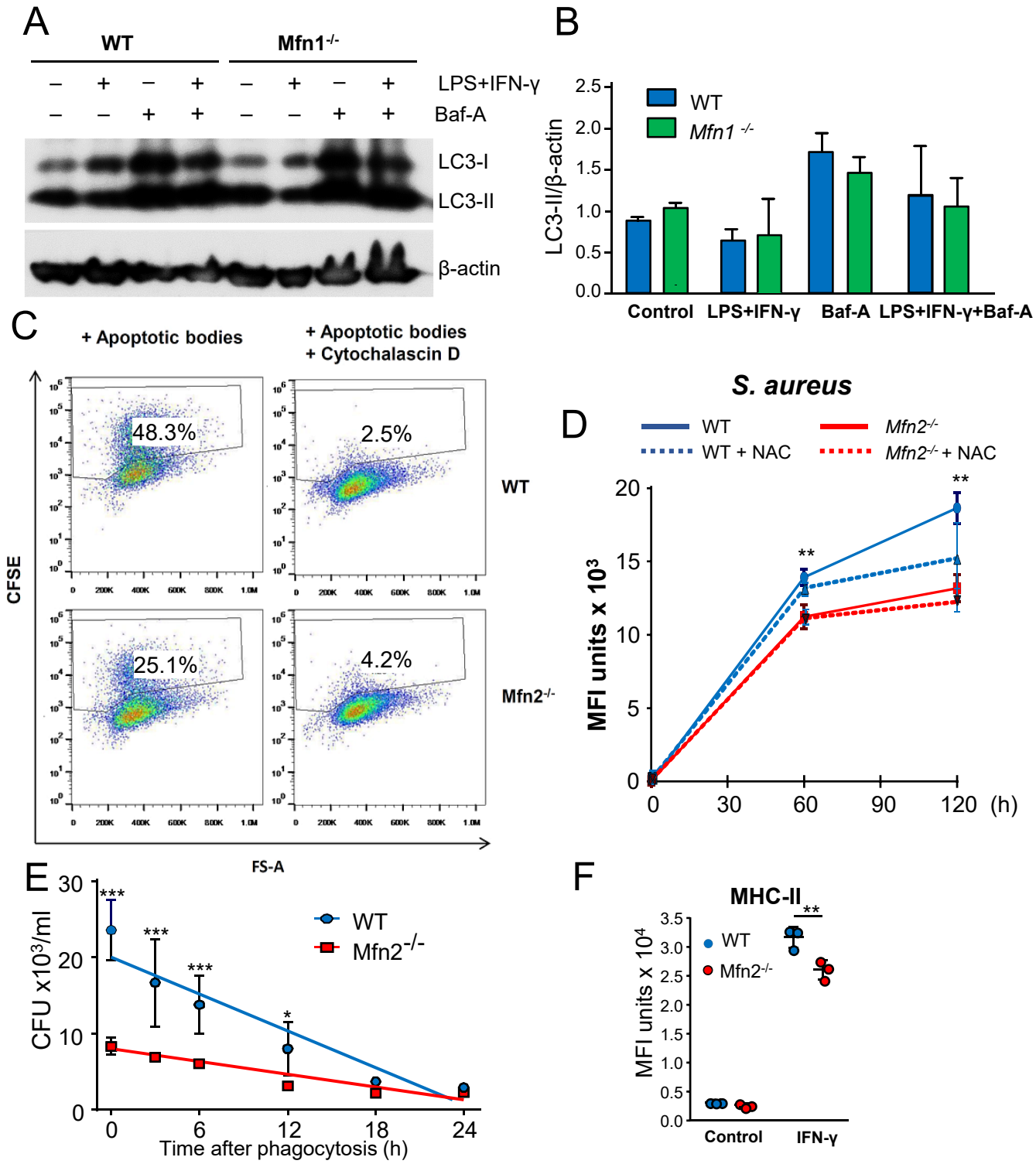

Figure S6. **Phagocytosis is impaired in cells lacking *Mfn2*$^{-/-}$. (A)** Autophagy was measured in control and *Mfn1*$^{-/-}$ macrophages by Western blot of the lipidated form of LC3 (LC3-II) in basal, or stimulated with LPS (10ng/ml), and/or bafilomycin A (BafA) at 50nM. **(B)** Quantification of three independent experiments. **(C)** WT and *Mfn2*$^{-/-}$ macrophages were untreated or cytochalascin D-treated (2µg/ml). Then macrophages were incubated with CFSE-stained apoptotic bodies from thymocytes in a relation of 10/1 macrophage. Phagocytosis was evaluated by flow cytometry as shown in the figure. **(D)** Phagocytosis at the specified time of pHrodo-conjugated *Staphylococcus aureus* by BMDM at 1mg/ml. When convenient, cells were treated for 1h with NAC (20nM) before bacteria were added and phagocytosis performed. **(E)** BMDM phagocyted *Aeromonas hydrophila* for 1h and then, non-phagocyted bacteria were removed with a gentamycin treatment (300µg/ml) for 1h. BMDM were incubated at 37ºC, and lysed at indicated times. The percentage of surviving bacteria was calculated based on counts. **(F)** MHC-II expression at the surface of IFN-γ (10ng/ml for 24 h) treated BMDM was measured by flow cytometry. Results are shown as mean ± SD from at least three independent experiments compared using two-way ANOVA: *p<0.05, **p<0.01, ***p<0.001. Related to Figure 5.

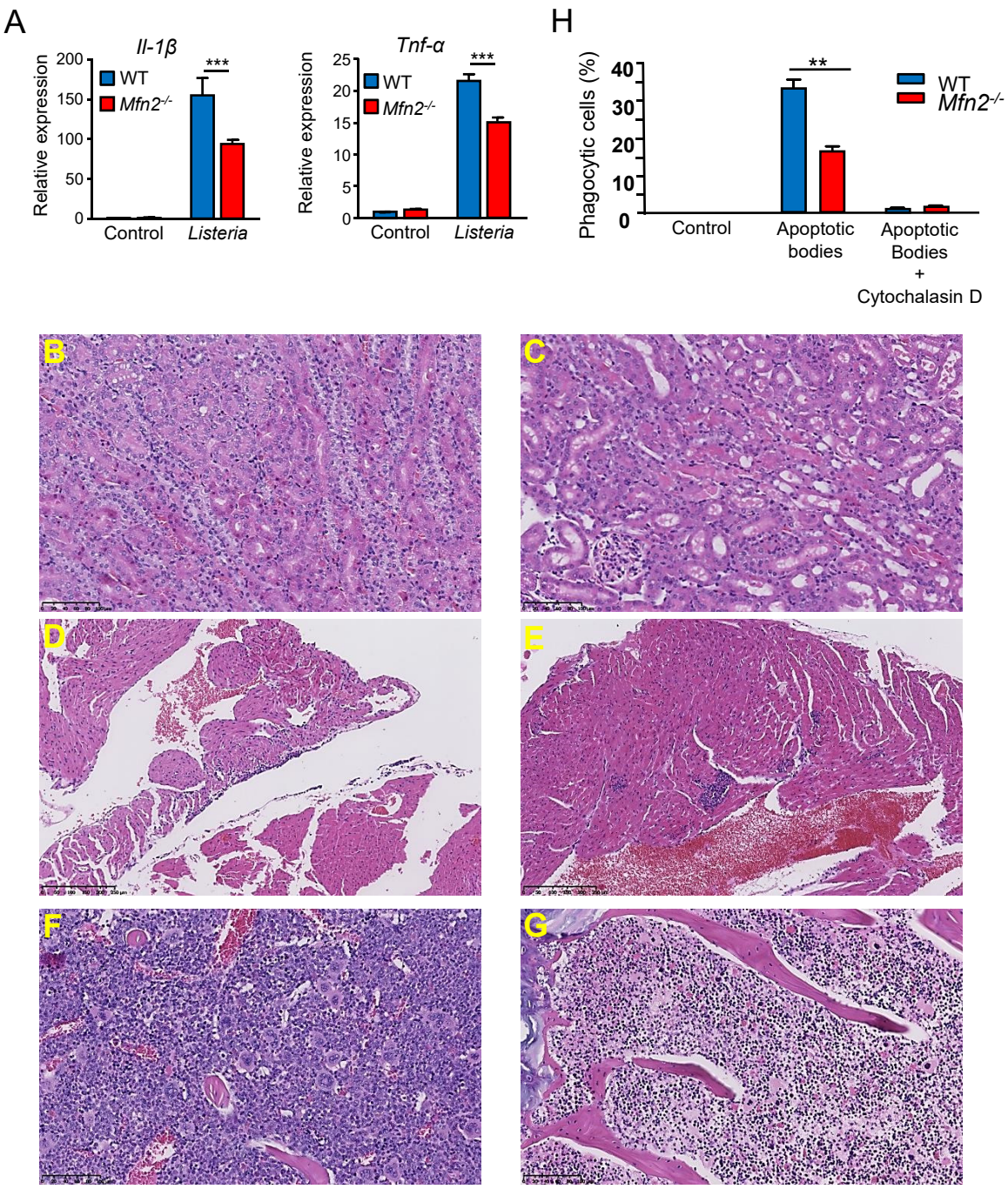

Figure S7. ***Mfn2$^{floxed;CreLysM}$*** **mice fail to be protected from *Listeria monocytogenes*, or LPS endotoxemia. (A)** mRNA expression from BMDM incubated *in vitro* with a MOI 5 *L. monocytogenes* for 6h. The results are shown as mean ± SD from three independent experiments compared using two-way ANOVA: ***p<0.001. Four WT and *Mfn2$^{floxed;\ Cre\text{-}LysM}$* mice were sacrificed 48h after LPS injection. **(B)** WT mouse, kidney: incipient necrosis/apoptosis in epithelial cells. **(C)** *Mfn2$^{floxed;\ Cre\text{-}LysM}$* mouse, kidney: focal areas of epithelial tubular cell necrosis. **(D)** WT mouse, heart: inflammatory infiltrate in the auricular pericardium. **(E)** *Mfn2$^{floxed;\ Cre\text{-}LysM}$* mouse, heart: myocardial multifocal purulent infiltrates. **(F)** WT mouse, sternum: bone marrow myeloid increase. **(G)** *Mfn2$^{floxed;\ Cre\text{-}LysM}$* mouse, sternum: bone marrow necrosis. **(H)** Control of phagocytosis of Fig. 7 D. Phagocytosis of apoptotic bodies was measured in BMDM control and treated with cytochalascin D (2µg/ml). Cells were incubated at a 1:10 macrophage:apoptotic bodies ratio for 1h and phagocytosis was evaluated by flow cytometry. Scale bar represents for B, C, F and G 100µm and for D and E 250µm. Results are shown as mean ± SD from three independent experiments compared using two-way ANOVA: ***p<0.01. Related to Figure 7.

Supplemental Table 1 for qPCR primer probes**.** Related to STAR Methods.

Oligonucleotides		
qPCR primer probe *18S* Forward	Merck KGaA	5´-TAGAGGGACAAGCGGCGTTC
qPCR primer probe *18S* Reverse	Merck KGaA	5´-CGCTGAGCCAGTCAGTCAGTGT
qPCR primer probe *Arg1* Forward	Merck KGaA	5'-TTGCGAGACGTAGACCCTGG
qPCR primer probe *Arg1* Reverse	Merck KGaA	5´-CAAAGCTCAGGTGAATCGGC
qPCR primer probe *Atf4* Forward	Merck KGaA	5´-CCGGAAATTCGTCAACGAGC
qPCR primer probe *Atf4* Reverse	Merck KGaA	5´-AGATCGTCCTAAAGGCCCCA
qPCR primer probe *Bip* Forward	Merck KGaA	5´-TGTGTGTGAGACCAGAACCG
qPCR primer probe *Bip* Reverse	Merck KGaA	5´-TAGGTGGTCCCCAAGTCGAT
qPCR primer probe *Chop* Forward	Merck KGaA	5´-CGACAGAGCCAGAATAACAGC
qPCR primer probe *Chop* Reverse	Merck KGaA	5´-AAGGTGAAAAGGCAGGGACTC
qPCR primer probe *Cytochrome c oxidase 1* Forward	Merck KGaA	5´-GCCCCAGATATAGCATTCCC
qPCR primer probe *Cytochrome c oxidase 1* Reverse	Merck KGaA	5´-GTTCATCCTGTTCCTGCTCC
qPCR primer probe *Fizz1* Forward	Merck KGaA	5´-TCTGCCCCAGGATGCCAACTTTGA
qPCR primer probe *Fizz1* Reverse	Merck KGaA	5´-GTCCAGTCAACGAGTAAGCACAGGC
qPCR primer probe *Gadd 34* Forward	Merck KGaA	5´-TACCCGGAGAGAAGCAGAA
qPCR primer probe *Gadd 34* Reverse	Merck KGaA	5´-GGCTTCGATCTCGTGCAAAC
qPCR primer probe *Hprt1* Forward	Merck KGaA	5´-ATCATTATGCCGAGGATTTGG
qPCR primer probe *Hprt1* Reverse	Merck KGaA	5´-GCAAAGAACTTATAGCCCCC
qPCR primer probe *IFN-β* Forward	Merck KGaA	5´-CAGCTCCAAGAAAAGGACGAAC
qPCR primer probe *IFN-β* Reverse	Merck KGaA	5´-GGCAGTGTAACTCTTCTGCAT
qPCR primer probe *Il-1β* Forward	Merck KGaA	5´-TGGGCCTCAAAGGAAAGAAT
qPCR primer probe *Il-1β* Reverse	Merck KGaA	5´-CAGGCTTGTGCTCTGCTTGT
qPCR primer probe *Il-6* Forward	Merck KGaA	5´CCAGAGATACAAAGAAATGATGG
qPCR primer probe *Il-6* Reverse	Merck KGaA	5´-ACTCCAGAAGACCAGAGGAAAT
qPCR primer probe *Il-12β* Forward	Merck KGaA	5´-TGGTTTGCCATCGTTTTGCTG
qPCR primer probe *Il-12β* Reverse	Merck KGaA	5´-ACAGGTGAGGTTCACTGTTTCT
qPCR primer probe *Il14* Forward	Merck KGaA	5´-TCCCAGGCTGTTAACGCGGT
qPCR primer probe *Il14* Reverse	Merck KGaA	5´-TCCCAGGCTGTTAACGCGGT
qPCR primer probe *Marco* Forward	Merck KGaA	5´- CGAATCTTTCCAACGCGTCC
qPCR primer probe *Marco* Reverse	Merck KGaA	5´-CAGAGCCACCTCCATAGCTG
qPCR primer probe *Mfn1* Forward	Merck KGaA	5´-CCCAGCAGCCCCGGATAATGC
qPCR primer probe *Mfn1* Reverse	Merck KGaA	5´-GGGTCGTCCACGTCAGCCTC
qPCR primer probe *Mfn2* Forward	Merck KGaA	5´-GCCAGCTTCCTTGAAGACAC
qPCR primer probe *Mfn2* Reverse	Merck KGaA	5´-GCAGAACTTTGTCCCAGAG
qPCR primer probe *Mkp1* Forward	Merck KGaA	5´-GGACAACCACAAGGCAGACAT
qPCR primer probe *Mkp1* Reverse	Merck KGaA	5´-GGCCTGGCAATGAACAAACA
qPCR primer probe *Mrc1* Forward	Merck KGaA	5´-CGCCCACCAGAGCCCACAAC
qPCR primer probe *Mrc1* Reverse	Merck KGaA	5´-TGCTCGCCAGCTCTCCACCT
qPCR primer probe *Msr1* Forward	Merck KGaA	5´-GTGCTGTCTTCTTTACCAGCA
qPCR primer probe *Msr1* Reverse	Merck KGaA	5´-ATGCTGTCATTGAACGTGCG
qPCR primer probe *Nadh 2* Forward	Merck KGaA	5´-CCTATCACCCTTGCCATCAT
qPCR primer probe *Nadh 2* Reverse	Merck KGaA	5´-GAGGCTGTTGCTTGTGTGAC
qPCR primer probe *Nos2* Forward	Merck KGaA	5´-GCCACCAACAATGGCAACA
qPCR primer probe *Nos2* Reverse	Merck KGaA	5´-CGTACCGGATGAGCTGTGAATT
qPCR primer probe *Opa1* Forward	Merck KGaA	5´-AGGACTTCTTCACTGCAGGTC
qPCR primer probe *Opa1* Reverse	Merck KGaA	5´-TCTGCAGCACCAGCTTCCGC
qPCR primer probe *Pecam-1* Forward	Merck KGaA	5´-CAACGCGGCAAACTAACCAA
qPCR primer probe *Pecam-1* Reverse	Merck KGaA	5´-CCGACTCCCCGTCAGCCAAT
qPCR primer probe *Sdha* Forward	Merck KGaA	5´-TGGGGAGTGCCGTGGTGTCA

qPCR primer probe *Sdha* Reverse	Merck KGaA	5´-CATGGCTGTGCCGTCCCCTG
qPCR primer probe *Sod1* Forward	Merck KGaA	5´-GGAACCATCCACTTCGAGCA
qPCR primer probe *Sod1* Reverse	Merck KGaA	5´-CCCATGCTGGCCTTCAGTTA
qPCR primer probe *Sod2* Forward	Merck KGaA	5´-AGGAGAAGTACCACGAGGCT
qPCR primer probe *Sod2* Reverse	Merck KGaA	5´-GCAGGCAGCAATCTGTAAGC
qPCR primer probe *Sxbp1* Forward	Merck KGaA	5´-CTGAGTCCGCAGCAGGTG
qPCR primer probe *Sxbp1* Reverse	Merck KGaA	5´-GGCAACAGTGTCAGAGTCCA
qPCR primer probe *Telomeric region* Forward	Merck KGaA	5´-GGTTTTTGAGGGTGAGGGTGAGGG TGAGGGTGAGGGT
qPCR primer probe *Telomeric region* Reverse	Merck KGaA	5´-TCCCGATTATCCCTATCCCTATCCCTA TCCCTATCCCTA
qPCR primer probe *Tgfβ* Forward	Merck KGaA	5´-GAGACGGAATACAGGGCTTTC
qPCR primer probe *Tgfβ* Reverse	Merck KGaA	5´-TCTCTGTGGAGCTGAAGCAAT
qPCR primer probe *Tnfα* Forward	Merck KGaA	5´-CCAGACCCTCACACTCAGATC
qPCR primer probe *Tnfα* Reverse	Merck KGaA	5´-CACTTGGTGGTTTGCTACGAC
qPCR primer probe *Wfs1* Forward	Merck KGaA	5´-CAGAGCTGGTCCCATGAAGG
qPCR primer probe *Wfs1* Reverse	Merck KGaA	5´-GGCAAGGCGTAGGTAGTGTT
qPCR primer probe *Xbp1* Forward	Merck KGaA	5´-CTGACGAGGTTCCAGAGGTG
qPCR primer probe *Xbp1* Reverse	Merck KGaA	5´-ACATAGTCTGAGTGCTGCGG
qPCR primer probe *Ym1* Forward	Merck KGaA	5´GCCAGCAGAAGCTCTCCAGAAGCA
qPCR primer probe *Ym1* Reverse	Merck KGaA	5´-GCACTGAACGGGGCAGGTCC
qPCR primer probe *β-2 microglobulin* Forward	Merck KGaA	5´-CTGACCGGCCTGTATGCTA
qPCR primer probe *β-2 microglobulin* Reverse	Merck KGaA	5´-CAGTCTCAGTGGGGGTGAAT